High Resolution Robust GPS-free Localization for Wireless Sensor Networks and its Applications

Thesis by

Mohammed Aquil Mirza

In Partial Fulfillment of the Requirements

For the Degree of

Masters of Science

King Abdullah University of Science and Technology

Thuwal, Kingdom of Saudi Arabia

December, 2011

The thesis of Mohammed Aquil Mirza is approved by the examination committee.

Committee Chairperson: Dr. Mohamed-Slim Alouini

Committee Committee: Dr. Basem Shihada

Committee Committee: Dr. Atif Shamim

King Abdullah University of Science and Technology

2011

ABSTRACT

High Resolution Robust GPS-free Localization for Wireless Sensor Networks and its Applications

Mohammed Aquil Mirza

In this thesis we investigate the problem of robustness and scalability w.r.t. estimating the position of randomly deployed motes/nodes of a Wireless Sensor Network (WSN) with out the help of Global Positioning System (GPS) devices. We propse a few applications of range independent localization algorithms that allows the sensors to actively determine their location with high resolution without increasing the complexity of the hardware or any additional device setup. In our first application we try to present a localized and centralized cooperative spectrum sensing using RF sensor networks. This scheme collaboratively sense the spectrum and localize the whole network efficiently and with less difficulty. In second application we try to focus on how efficiently we can localize the nodes, to detect underwater threats, without the use of beacons. In third application we try to focus on 3-Dimensional localization for LTE systems. Our performance evaluation shows that these schemes lead to a significant improvement in localization accuracy compared to the state-of-art range independent localization schemes, without requiring GPS support.

ACKNOWLEDGMENTS

I would like to sincerely thank my supervisor Dr. Mohamed Slim Alouini for his continuous guidance and encouragement throughout the course of this work. His enthusiasm and valuable feedback for research made my study very enjoyable and exciting and ultimately fruitful with rich experience. I would also like to thank him for providing me with an amazing research environment.

I thank my parents for their continuous encouragement and my siblings for bearing with me for my negligence towards them during this journey and their deep moral support at all times.

Lastly, I would like to thank the people at KAUST, Thuwal, Makkah Province, Saudi Arabia for providing support and resources for this research work.

TABLE OF CONTENTS

LIST OF ILLUSTRATIONS

Chapter 1

INTRODUCTION

GPS-free Localization in wireless communications has been an open problem till date. Making the localization scheme robust and scalable is another issue that this thesis tries to tackle. The implemented method relies on two well-established techniques - localization and spectrum sensing [1-3]. Localization refers to the process of discovering the position of a particular signaling device. Localization algorithms implemented within sensor networks are proposed to provide node location information. These algorithms could be divided into two classifications: range-based and range-free. Range-based algorithms rely on point-to-point distance estimates (range) or angle estimates in order to provide location information. Examples of those are ToA (Time of Arrival), TDoA (Time-Distance of Arrival), AoA (Angle of Arrival) and RSS (Received Signal Strength) [4]. In 3-D, range-free algorithms assume that distance/angle estimates are nonexistent (or invalid, if they do exist), and thus they exhibit no reliance on such estimates. Instead, range-free algorithms make use of the radio connectivity information each sensor node possesses (i.e. each node possesses information about its own position) or rely on the capability of sensor nodes' own sensing abilities.

In this thesis, we present three independent applications, from there different

fields (spectrum sensing in urban areas, underwater localization and femtocells localization), where localization plays a vital role. Localization will not only resolve the problems of cost efficiency (GPS-free) but also resolves the problems of fault detection (least probability of false alarm). We show that sensor nodes localization is very demanding, where in the sensor nodes are deployed, whether it be underwater sensor network or 4G network communications (femtocells). Localization thus surrounds the sensor network. We give a brief overview of these applications below.

In our first application, we address and simulate a Radio Frequency (RF) sensor network for a cooperative spectrum sensing and localization scheme. The proposed scheme LCC (Localized and Centralized Cooperative) Spectrum Sensing integrates a Wavelet based Multi-Resolution Spectrum Sensing (MRSS), an N-bit hard combination technique for cooperative decision making and a Received Signal Strength (RSS) based localization algorithm to detect the availability of frequency bands and the location of the usable base station. We develop an N-bit hard combination technique and compare its performance to a traditionally used 2-bit hard combination for cooperative sensing. The key idea is to design a novel RF sensor network based cooperative wideband spectrum sensing and localization scheme by using a wavelet based MRSS and RSS Localization techniques which were originally proposed for cognitive radio applications. The performance evaluations are also done to show the different detection accuracies for varying parameters such as number of sensor nodes, Signal to Noise Ratios (SNR) and number of averaged Power Spectral Densities (PSD). The proposed scheme improves the problems of shadowing, fading and noise. In addition, the RSS based localization technique has been shown to be an acceptable means of estimating the position of the available transmitter.

Cognitive radio has been known as a novel paradigm for improving the utilization of the precious natural resource radio spectrum. Spectrum sensing is a key component in cognitive radio for detecting spectrum holes, which are the spectrum channels

not used by any primary user. Previous work [1] shows that opportunistic spectrum sharing promise a high gain in wireless capacity. To realize this gain, a method of accurately identifying spectrum holes or white space is needed. Frequencies allocated to a broadcasting service but not used locally are called white spaces [1]. Recently, the Federal Communication Commission (FCC) issued the final rules for implementing the usage of white spaces for unlicensed wireless devices. The decision to allow this was met with wide interest due mainly to the many advantages provided by enabling wireless communications in white space, such as the vastly improved range, the capability to penetrate through obstacles, and much higher speeds.

However, such an implementation would not be without its problems, which mainly arise when examining the spectrum offered by white space. The issue in question is that even though television is largely digitized and thus freeing more spectrum, the available white space is already being utilized by several licensed users (e.g. wireless television cameras, microphones), and thus interference with such users would be highly probable [4] . The difficulty of assigning proper buffer zones in order to avoid said interference is what led the FCC to implement in its final ruling very strict emission guidelines that prevent the direct use of 802.11 in a single channel, which would effectively make the new white space spectrum unusable for Wi-Fi technologies [3, 4].

An efficient underwater localization is portrayed too. Seaweb is an acoustic communication technology that enables communication between sensor nodes. Seaweb interconnects the underwater nodes through digital signal processing (DSP)-based modem by using acoustic links between the neighbouring sensors. In this thesis, we design and investigate a global positioning system (GPS)-free passive localization protocol using seaweb technology. This protocol uses the range data and planar trigonometry to estimate the positions of the discovered nodes. We take into consideration the small displacement of sensor nodes due to watch circles (like tides) and

placement of sensor nodes on non-uniform underwater surface, for precise localization. Once the nodes are localized, we divide the whole network field into circular levels that minimizes the traffic complexity and thereby increases the lifetime of the sensor network field. We then form the mesh network inside each of the circular levels that increases the reliability. The algorithm is designed in such a way that it overcomes the ambiguous nodes errata and reflected paths and makes the algorithm more robust. The synthetic network geometries are so designed which can evaluate the algorithm in the presence of perfect or imperfect ranges or in case of incomplete data. A comparative study is made with the existing algorithms which proves our newly proposed algorithm to be more effective in terms of localization and energy consumption.

Three-dimensional Localization in Long Term Evolution (LTE) of 4G networks is one of the important problem that we try to solve here. Femtocells provide an efficient solution to overcome the indoor coverage problems and also to deal with the traffic within Macro cells. The possibility of localizing femtocell subscriber stations based on the timing ranging advance parameter (TRAP), obtained from E-UTRAN (Evolved UMTS Terrestrial Radio Access Network), within the network signal internals is challenging and is studied throughout in this thesis. The principle approach to localization based on Euclidean distances from multiple base stations is outlined. We investigate the specifications of the timing parameters or TRAP used for air interface of 4G network as they relate to calculating the subscriber distances. Computer simulation is used to demonstrate the localization accuracy using multiple base station networks when estimating likely locations of femtocell subscribers stations on a two-dimensional coordinate mapping system. However, we further extend our simulations to demonstrate expected location accuracy of subscriber stations, for multiple base station networks, on a three dimensional coordinate mapping scheme. The possibility of error-fixes shows eight times greater accuracy than in previous results is expected

to achieve by applying timing advance techniques to Global System for Mobile communications networks, by using a two-dimensional coordinate mapping scheme. We later compare our study with the effect of global positioning system (GPS) by using a three-dimensional coordinate mapping scheme, which is predicted to give an 72.4 cms accuracy of subscriber station location.

1.1 Related Work

GPS-free localization is very challenging and requires precise and accurate position location of the nodes, in order to avoid critical circumstances. Some of the applications of localization may include volcanic eruption, erathquate monitoring, harbor monitoring, and so on. Some recent works try to find the applications of localization in the upcoming fields, like spectrum sensing and Long Term Evolution (LTE) Technologies, but suffers from some drawbacks.

In [4] authors require the Effective Isotropic Radiated Power (EIRP) information for localization. In practical scenarios, this information is not available. In [4, 8] authors uses MRSS technique with soft combination schemes for spectrum sensing. This requires wider bandwidth and requires more overhead. In [15] a technique incorporating the time synchronization between the two nodes without considering the notion of reflected paths, which increases the error exponentially. The complexity of this scheme [17] is not low, it may result in poor energy efficiency. The basic approach to localization based on Euclidean distances from multiple base stations is studied in [32], which proves out to be very energy expensive. Moreover, transformation of a binary image in linear time are not widely used in practice.

We try to resolve the problem and issues of the above mentioned papers come up with novel and energy efficient techniques for localization. This is further discussed in the upcoming chapters.

1.2 Contributions

The major contributions for the following chapters are defined here briefly. In chapter 2, we present a localized cooperative wide band spectrum sensing technique. In this, we try to achieve the following goals. Firstly, we localize the RF sensor nodes to effectively find out the EIRP of the transmitter (primary user). To achieve this we follow RSS approach. Secondly, we devise a mechanism (Using RF Sensor nodes) to efficiently sense the spectrum for white spaces and we use a combination of Wavelet based MRSS and N-bit hard combination to achieve this. Thirdly, we try to cooperate among the RF sensor nodes and BS to increase the probability of detection, P_D. We also try to overcome the problems of fading and shadowing by averaging power spectral densities (PSD's).

In chapter 3, we present a GPS-free underwater localization scheme. We mostly focus on speed of sound profile and try to achieve the following goals during the design of our protocol. Firstly, we consider the fact that speed of sound usually varies from 1480 m/s to 1520 m/s, i.e, having a deviation of $+1.3\%$ or -1.3%. This is taken into consideration by using Munk's Canonical formula. Secondly, we consider transmitted/reflected paths, which can result into absorption and scattering, that reduces the intensity of sound energy. Thirdly, we take into account the node position or depth variance, as it is possible that two nodes are located at uneven surfaces and both of them have a horizontal and a slant range. Then, we account for current/waves circles. This is mainly due to tides can replace the fixed/stationary transducers, thereby causing deviations. Finally, we tackle the problem of dilution of precision (DOP), which occurs when the distance between the two referenced nodes is very close.

In chapter 4, we present a 3-Dimensional localization scheme for femtocell subscribers. Firstly, we try to find the possibility of geolocalization of femtocell subscriber stations based on from E-UTRAN (Evolved UMTS Terrestrial Radio Access

Network). We then calculate timing ranging advance parameter (TRAP) for 4G-Femtocell networks. This information is mostly used during the time synchronization of uplink and downlink channels. We also study the range-approximations for calculation of the 3-Dimensional distance between eNodeB (Femtocell Base Station) and User Element (UE).

Chapter 2

LCC: Localized and Centralized Cooperative Spectrum Sensing

Localization also plays a significant role in the field of spectrum sensing. Sensing the transmission power of the primary user (PU) and informing the secondary users (SU), so that SU do not interfere with PU, is a critical issue. Sensing the spectrum band with sensor nodes is also very challenging, as sensors are low power devices. In [5,6] a technique incorporating the time synchronization between the two nodes without considering the notion of reflected paths, which increases the error exponentially. However, the complexity of this scheme [5] is high which may result in poor energy efficiency. Moreover, this scheme is very difficult to extend this scheme to larger networks. In particular, the number of beacon nodes is set to three in the paper; however, if more than one beacon node is added, then not only program changes are needed for both beacon and ordinary nodes, but also the computational complexity will increase exponentially. However, we try to overcome the problem of reflected paths and watch circles in our scheme and the proposed scheme does not require time synchronization in the network. In [5], the network calculations are implemented by using the ordinary sensor nodes, and we reduce this complexity by incorporating

seaweb/GB communication. In [7], an application of sensor deployment in the Unet'08 seatrial is studied. A fixed speed of sound profile is considered which increases the localization error. This scheme does not take into consideration the displacement of the nodes on the sea surface. We overcome this problem by using Munk's canonical formula [8] and the finite difference linearization and law of cosines.

In this chapter, we propose a localized and centralized cooperative spectrum sensing scheme which tries to overcome the aforementioned problems of beacon or anchor free localization. Fig. 2.1 shows the two step working principle of our proposed scheme where the child nodes (shown in blue) work collaboratively to sense the TV bands and send the data to and parent node (shown in red). The parent node inturn make the decision for presence of signal by the collaborative results from the sensor nodes. Fig. 2.2 shows the block diagram of the proposed RF sensor network-based cooperative wideband spectrum sensing and localization. The function of each of the block is explained as follows. Once all the nodes are deployed in the network they try to localize and sense the environment. RF sensor networks localize by means of averaging RSS from the neighboring nodes. After localization is completed, all the sensors sense the environment for the detection of signals transmitted from the various Transmitters or Transmitter Access Points (TAP) and do a coarse resolution sensing to obtain the wide spectrum of frequencies. An N-bit hard combination combines the coarse resolution sensing to detect the presence of signals in the respective or interested band of spectrum. Fine resolution sensing is then applied to these frequency bands to narrow down the spectral bands of signals in the air and thus calculate the frequency band. The sensor nodes then try to estimate the position and equivalent isotropically radiated power (EIRP) of the transmitter emitting these signals. EIRP is calculated by using the linear equation 2.2. The proposed cooperative wideband spectrum sensing and localization scheme uses wavelet-based MRSS technique in the coarse and fine resolution sensing blocks.

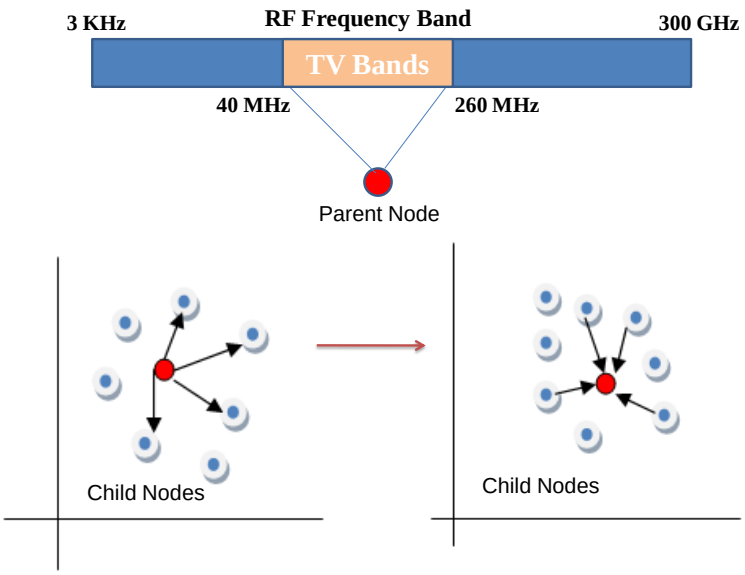

Figure 2.1: Working principle of the proposed scheme

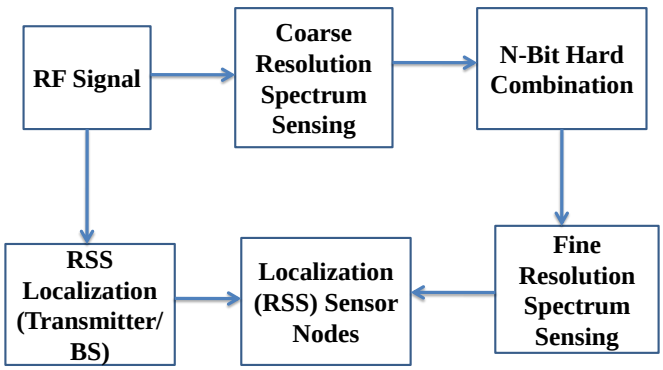

Figure 2.2: Functional block diagram of the proposed cooperative wideband spectrum sensing

2.0.1 Network Topology

A parent/master node is assigned among the sensor nodes that act as a central computation node. The master node applies a coarse resolution spectrum sensing to the whole bandwidth of interest and determines N-thresholds, which divides the frequency range into 2^N-regions. Based on the frequency range, the value of N is determined by the parent node. If there is a large frequency band to be sensed then N is large: the higher the value of N, the higher the probability of detection (refer to Section III). However, in this chapter, we compare 2-bit, 3-bit and 4-bit (i.e. N = 2, 3 and 4 respectively) hard combination schemes for evaluations. Once the parent node does the coarse resolution of the interested spectrum it inform all other child nodes about the divisions of thresholds and regions of energies (of this spectrum). After applying the thresholds, the child nodes evaluate the frequency bands in which the sensed signal/energy exceeds the first threshold and thereby determines its region. The child nodes then send an N-bit value to the parent node. The parent node determines the bands on which the fine resolution sensing needs to be applied by using the N-bit combination scheme. The nodes that sense the highest energies on the determined spectrum bands will only apply fine resolution sensing. Next each sensor node applies the N-threshold values that are below the maximum observed signal energy sensed by the coarse resolution sensing in the specified spectrum band. This in turn allows the nodes to calculate the frequency bands of the signals in the region.

2.0.2 Received Signal Strength

The RSS-based localization technique introduced in [4] requires the knowledge of EIRP of the transmitter. But here we show that our proposed scheme calculates the EIRP information as a function through least squares estimation. In this proposed scheme we assume that the transmitter antenna is omni-directional. The nodes (at least three) that know their position, with respect to the base station (which is set as

origin point), must calculate the RSS values from the signal of interest. Once these nodes are localized through triangulation, the other nodes in the network will then localize with respect to these known locations. The RSS value of the y^{th} node is equal to the ideal received power, P_y, defined by the equation

$$P_y = C_y \frac{P_t}{d_y^{\alpha}} \tag{2.1}$$

where P_t is the EIRP of the transmitter and C_y is assumed to be constant for simplicity (equals to 1) representing the antenna height and gain, and α (varies from 3 to 6) is the path loss exponent and d_y is the distance between the transmitter and the y^{th} node, given as $d_y = \sqrt{(x - x_y)^2) + (y - y_y)^2}$ where (x, y) is the position of the transmitter and (x_y, y_y) is the position of y^{th} node to be determined. Once the value of d_y is substituted in (1) and takeing $2/\alpha$ power on both sides we obtain,

$$(\frac{C_\alpha}{P_y})^{2/\alpha} = \frac{(x - x_y)^2) + (y - y_y)^2}{(P_t)^{2/\alpha}} \tag{2.2}$$

extending the above equation for all nodes it yields the following matrix equation:

$$\begin{bmatrix} 2x_1 & 2y_1 & \frac{C_j{}^{\frac{2}{\alpha}}}{P_1} & -1 \\ 2x_2 & 2y_2 & \frac{C_j{}^{\frac{2}{\alpha}}}{P_2} & -1 \\ \vdots & \vdots & \vdots & \vdots \\ 2x_m & 2y_m & \frac{C_j{}^{\frac{2}{\alpha}}}{P_m} & -1 \end{bmatrix} \begin{bmatrix} x \\ y \\ P_t^{\frac{2}{\alpha}} \\ x^2 + y^2 \end{bmatrix} = C$$

where $C = \begin{bmatrix} x_1^2 + y_1^2 \\ x_2^2 + y_2^2 \\ \vdots \\ x_m^2 + y_m^2 \end{bmatrix}$

Using the least squares method we can solve this linear equation. The linear equation provides the position of transmitter and EIRP. The shadowing (fading caused by

obstacles) effect is included by using log-normal path loss model, which is given by

$$P_y = C_y \frac{P_t}{d_y^a S_y} \tag{2.3}$$

where $S_y = 10^{0.1 f_y}$ is a log-normal random variable and f_y is a Gaussian random variable with zero mean and σ^2 variance. To minimize the effect of shadowing, RSS values are averaged and are given by

$$P_y = \frac{1}{S} \sum_{i=1}^{s} P_{y_i} \tag{2.4}$$

where S is the total number of samples and P_{y_i} is the i_{th} sample RSS value at y_{th} node in dBm.

Multi-Resolution Spectrum Sensing (MRSS)

This energy detection scheme is used at two different spectrum resolution sensing: coarse spectrum sensing and fine spectrum sensing. MRSS is used in coarse spectrum sensing to sense the entire bandwidth, which provides a quick overview of the spectrum. In fine resolution we apply MRSS to a specific band of interest. By using this we do not sweep for entire bandwidth of the system continuously, therefore sensing time and energy consumption of the RF sensors are greatly reduced. However, there is a tradeoff between energy consumption and correct P_D, when sweeping the whole TV band of spectrum.

Wavelet-Based MRSS

Fig. 2.3 shows the block diagram of wavelet based MRSS. In this technique we change the pulse width/duration of the generator and the sinusoidal functions of the frequencies to sense the spectrum with different resolutions. Generally, we change the pulse width, T_g, and the sweeping frequency, f_{sweep} to obtain the different sensing

resolutions. A small T_g or large f_{sweep} provides coarse resolution sensing (Fig. 2.4) whereas, a large T_g and a small f_{sweep} provides fine resolution. The pulse width is multiplied by the cosine and sine frequency having the same frequency as the inspected frequency. Then these obtained results are multiplied by the RF signals. Once these signals are multiplied they are integrated and digitized. The output of the correlator is squared and summed. The square root of this sum gives the spectral density function, P_k. Averaging P_k reduces the noise factor and makes signals more accurate and improves the estimation performance.

The mathematical working model is explained as follows; The input signal is $x_{(t)}$ is multiplied with the inphase and quadrature components as

$$x_{I,k}(t) = x(t)cos(2\pi f_k t) for k = 0, ..., K$$

$$x_{Q,k}(t) = x(t)sin(2\pi f_k t) for k = 0, ..., K \tag{2.5}$$

where $f_k = (f_{start} + k f_{stop})$ is the k^{th} observed frequency and $K = Round(f_{stop} - f_{start})$ is the number of observed frequency values.

The output of the integrator or analog correlators for every f_k is then given as

$$z_I(t) = \frac{1}{T_n} \int_{kT_n}^{(k+1)T_n} [r(t)g(t)cos(2\pi f_k t)]dt$$

$$z_Q(t) = \frac{1}{T_n} \int_{kT_n}^{(k+1)T_n} [r(t)g(t)sin(2\pi f_k t)]dt \tag{2.6}$$

Finally, we obtain the power spectral density as

$$P_k = \sqrt{z_I^2(kT_n + z_Q^2(kT_n)} \tag{2.7}$$

where $z_I(kT_n)$ and $z_Q(kT_n)$ are the discrete values of $z_I(t)$ and $z_Q(t)$

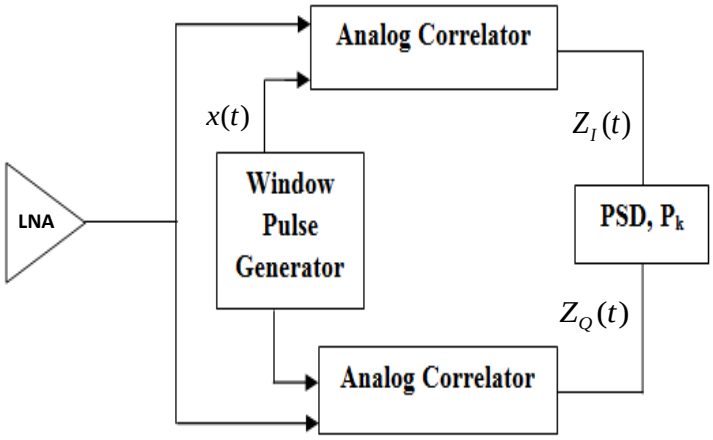

Figure 2.3: Multi-Resolution spectrum sensing

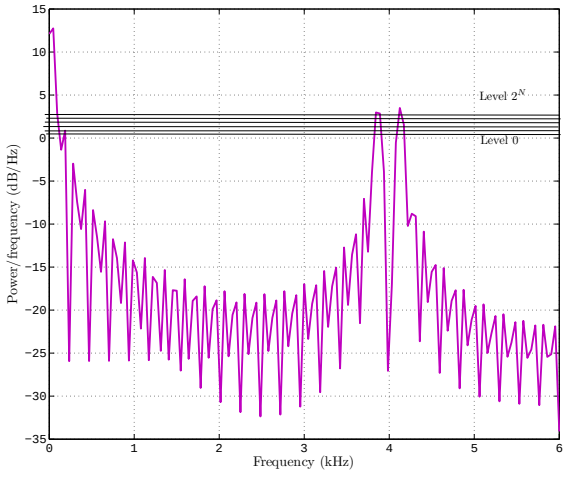

Figure 2.4: Output of the coarse resolution spectrum sensing

Cooperative Spectrum Sensing

The cooperation of sensors is affected by environmental noise (assumed as white Gaussian), shadowing and fading which in turn makes the RSS very low and this can prevent the nodes from sensing the signal of interest. For a very low signal to noise ratio (SNR), the signal of interest is not detected. The idea of cooperation in sensor networks is to minimize the effect of shadowing, fading and noise and to collaborate between the nodes in deciding the spectrum band used by the transmitters emitting the signal of interest. Nodes send their test statistic or an N-bit value to the parent node, which in turn makes a decision for the presence of a signal. We show in the next section that as the number of nodes increases the probability of missed detection decreases and the probability of detection increases.

There are two forms of cooperation in spectrum sensing namely hard combination and soft combination. These forms are more commonly known as decision fusion or data fusion respectively. The only difference between these two is the type of information sent to the parent node. In hard combination we send an N-bit value (say 3 bits for 3-bit combination) and in soft combination the sensor nodes sends the test statistic to the parent node. The major advantage of hard combination is that it requires only one bit of communication overhead and low-bandwidth for the transmission. The hard combination and soft combination techniques are explained in detail in [5].

N-bit Hard Combination Scheme

The N-bit combination scheme has an advantage of lower overhead as compared to using 2-bit hard combination. The main idea behind this scheme is to divide the whole range of observed frequency signals into more than 2^2 regions and to assign different weights to the regions. This gives an advantage of nodes that observe higher energies in the upper regions have greater weights than those in the lower energies. Authors

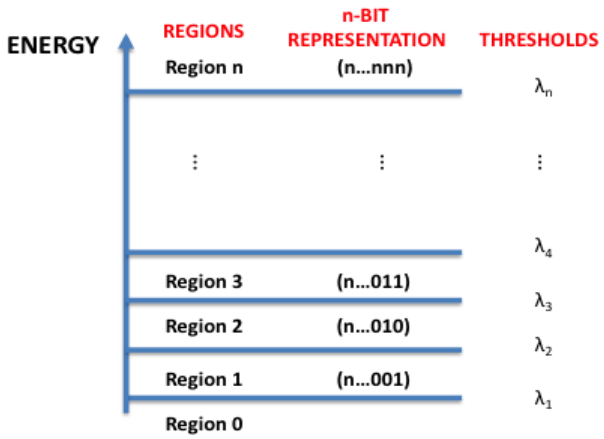

Figure 2.5: Energy regions for the proposed N-bit hard combination scheme with respective thresholds (n represents N)

in [8, 10] show that 2-bit outperforms 1-bit hard combination scheme and have less communication overhead when compared to traditional combination schemes, where the test statistics are sent to the parent node. However, in our scheme the nodes send an N-bit value to the decision maker node (parent node) instead of the test statistic, which causes less overhead.

Figure 2.5 and Table 2.1 show the weights assigned for the different levels of energies for an N-bit combination scheme. The thresholds divide the whole range of energies into n-regions and for each region we assign the weights defined as

$$w_0 = 0$$

$$w_1 = 2$$

$$\vdots$$

$$w_{n-1} = L$$

$$w_n = L^2$$

where L is a design parameter [8].

Thresholds of the N-bit hard combination is determined by using the Neyman-Pearson Criterion, where the value of probability of false alarm P_{FA} is fixed to some value and the probability of detection P_D is maximized. The P_{FA} is defined as follows.

Table 2.1: Respective thresholds and corresponding P_{FA} values

Threshold	P_{FA} **Values**
λ_1	P_{FA}
λ_2	$\beta_2 P_{FA}$
λ_3	$\beta_3 P_{FA}$
λ_4	$\beta_4 P_{FA}$
$\vdots$	$\vdots$
λ_n	$\beta_n P_{FA}$

$P_{FA}\% =$

$$\frac{\text{Number of} f_k \text{false alarm more than} N_{sim}/2 \text{times}}{Round[(f_{stop} - f_{start})/f_{sweep}]} \times 100 \tag{2.8}$$

This criterion is useful when the a priori probabilities and the cost assignments for each possible decision are difficult to assign. Table 1 shows the strategy to choose the values of P_FA. The coefficient, β_n is defined as $\beta_n = 10(n-1)$ and $\beta_1 = 1$ for simplicity. The presence of signal is determined by $\sum_{r=1}^{n} E_r w_r \geq N$ where N is the number of nodes in the network and E_r is the energies observed in region r and w_r is the weight assigned to the particular region. If the weighted sum in Equation 7 is greater than N then the signal is present in that particular region. Weights are defined as follows: If any of the nodes observes a signal in region n, with no detected signals in other regions then the signal is present. Similarly, if any of the nodes observe a signal in region $n-1, n-2 \cdots 1$ with no other detected signals, and then the signal is present in the region. This can be seen from Table 2, which shows the weights and thresholds for different values and for different regions.

2.1 Simulation Results

In this section we discuss the simulation setup for our proposed scheme and its comparison with traditional techniques. We try to simulate the model by varying the

Table 2.2: Weight Assignment for Different Regions

Region	**No. of Nodes required to declare presence of signal**	**Weight Assigned**
0	-	$W_0 = 0$
1	60 % of nodes	$W_1 = 1.66$
2	50 % of nodes	$W_2 = 2$
3	40 % of nodes	$W_3 = 2.5$
⋮	⋮	⋮
4	1 % of nodes	$W_n = 100$

averaged power spectral densities (PSDs), number of nodes localized and its respective normalized localization error. We also study the effect of standard deviation of the Gaussian random variable for the effect of shadowing.

2.1.1 Simulation Setup

In the determination of the thresholds for the different energy regions for coarse resolution and fine resolution a window is generated. The effect of various types of windows (like Flattop, Hamming, Kaiser and Rectangular) is studied by measuring the energy level at 100 MHz for the coarse resolution block and calculating the detection margin, D_M above the N^{th} threshold at the child node, while the number of PSD's is 15 and SNR is equal to 0 (the values are selected on trial and error basis).

D_M=(Observed energy at 100 MHz)-N^{th} threshold value

The simulation results proves that rectangular window provides the best detection margin at a value of 7.862 dB above the N^{th} threshold. Using a Kaiser window, a very close detection margin of 7.3 dB is obtained. The values for other windows fall much below than these windows. Based on the simulated results a rectangular window is used throughout the simulations. The simulation results are shown in Fig. 2.6.

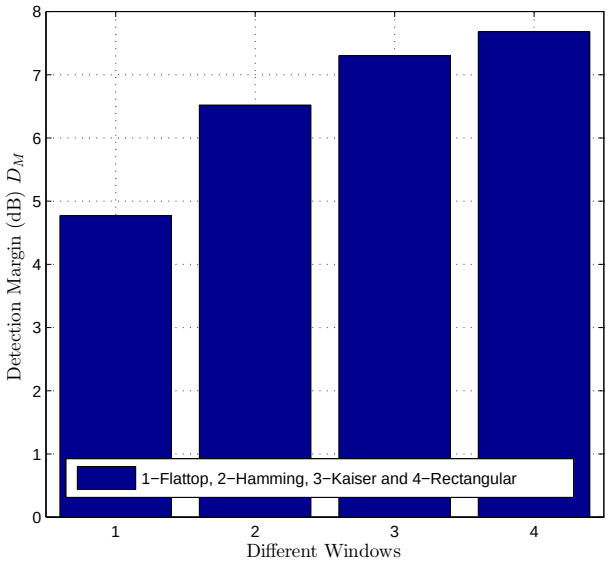

Figure 2.6: Detection Margin versus Window Type

2.1.2 Comparison with Traditional Scheme

In Fig. 2.7, we make the comparisons with traditional 2-bit hard combination and N-bit (3-bit and 4-bit) hard combination. The figures show the detection percentage versus SNR. The comparison shows that when the SNR is between -25 dB to -19 dB, the traditional hard combination schemes perform better. This is because one node sensing the energy above the threshold is already enough in declaring that there is a presence of signal. However, in Fig. 2.8, we can see that the probability of false alarm (which we want to be low), P_{FA} percentage is higher for 2-bit hard combination and decreases as N increases.

2.1.3 Effect of Number of Averaged PSDs

Fig. 2.9 shows the number of averaged PSDs over detection percentage as a function of number of nodes when the SNR is maintained at -15 dB. Note that the detection percentage for the plots indicates the percentage of correct decisions out of 10,000 instances of the simulation done in Matlab (Monte Carlo approach). The results

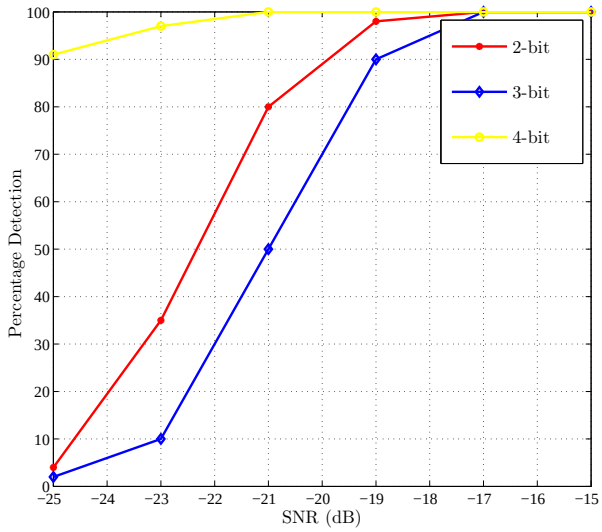

Figure 2.7: Comparison of N-bit hard combination scheme (Percentage Detection vs SNR).

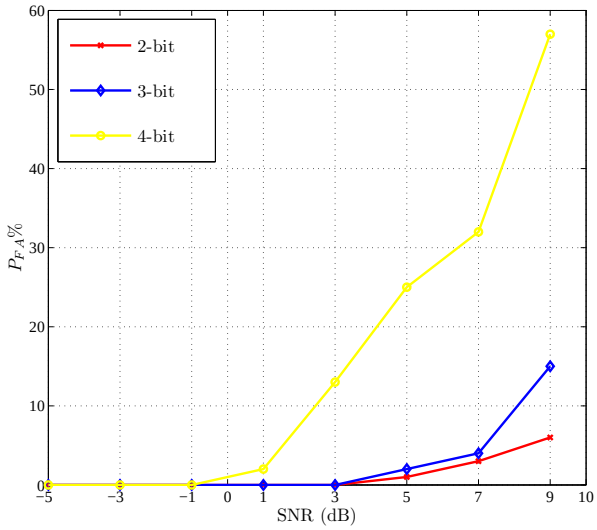

Figure 2.8: Comparison of N-bit hard combination scheme (P_{FA} vs SNR).

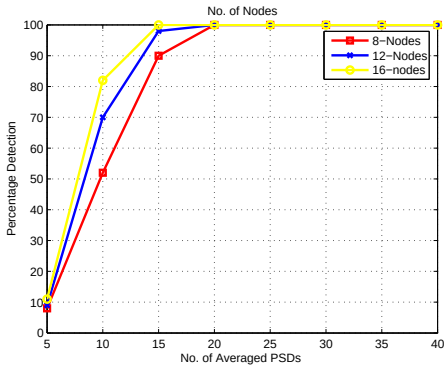

Figure 2.9: Percentage detection vs Averaged PSDs, $N = 4$

show that as the number of nodes increases, the accuracy for detecting the presence of transmission in a given frequency increases. This can be attributed to the fact that the more nodes that are sensing the spectrum, then there is more information that can be considered in making the decision. However, at some point, adding more nodes do not increase the information needed to make the decision so the improvement stops (somewhere after 15 to 20 nodes). However, this is limited to this specific setup of ours. In fact, this mainly depends upon kind of network area being selected. Similarly, in Fig. 2.10, if the signal-to-noise ratio is relatively high, the detection accuracy is also higher because the information sent among the nodes will be more accurate as well.

2.1.4 Effect of Number of Nodes

We then study the effect of number of nodes in the network field. As sensors are prone to failures due to quick drainage of energy, we incorporate the cooperative wideband sensing for increasing the lifetime of the network. It is shown in Fig. 2.11 that for sensor networks with more than 6 nodes, increasing the number of nodes increases the detection accuracy and even performs better with less PSD's. Having to average less PSD's helps the sensor nodes to conserve energy and thus helps prolong the lifetime of the sensor network.

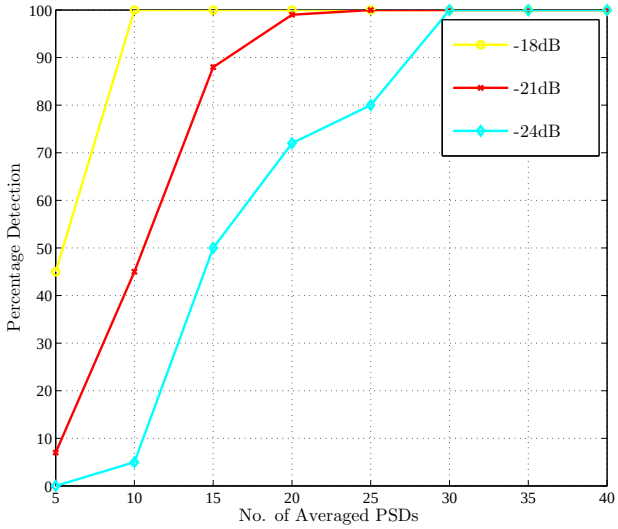

Figure 2.10: Percentage detection vs Averaged PSDs, $N = 4$

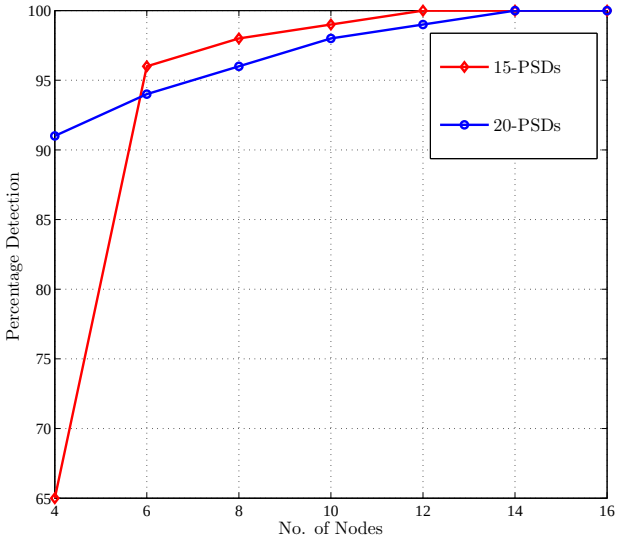

Figure 2.11: Percentage detection vs No. of Nodes, $N = 4$

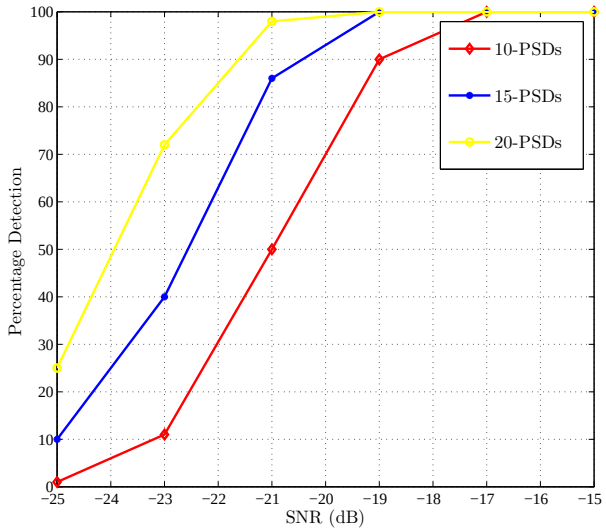

Figure 2.12: Percentage detection vs SNR, $N = 4$

2.1.5 Effect of SNR

Fig. 2.12 shows the effect of SNR on detection percentage for three different number of PSD's averaged values when 10 nodes participate collaboratively and cooperatively in the wideband spectrum sensing. We studied the effects of SNR as an energy detector (PSDs) that depends on its levels. The effect of SNR is shown in Fig. 2.12 for fixed number of averaged PSDs, when only 15 nodes are participating in sensing. This figure shows that the proposed scheme works better when there is a high SNR.

2.1.6 RSS Based Localization Results

The last part of the simulation focuses on the evaluation performance of the RSS-based scheme on Mean Square Error (MSE) for detecting the distance between the sensor nodes and transmitter.

$$\Delta_{MSE} = \frac{1}{N}\sum_{n=1}^{N}\sqrt{(x - x_{cal,n})^2 + (y - y_{cal,n}^2)} \tag{2.9}$$

Where (x,y) is the true position of the transmitter and (xcal,n, ycal,n) is the nth

calculated position and N is the number of simulation runs. In this simulation, we used 10,000 realizations and then by averaging we obtain the results. The results show that as the number of nodes and samples increases the MSE is decreasing. These results are depicted in Fig. 2.13 below. Furthermore, increasing the shadowing effect by increasing sigma (standard deviation) drastically increases the MSE. In Figure 2.14 it shows the original received signal strength indication (RSSI) versus the predicted/estimated RSSI. It can be seen here that there is a small deviation between the original and the calculated (weight predicted) positions of the nodes indicating that the RSS-based localization is working considerably well.

In this chapter, we propose a novel technique of how localization can be incorporated in wideband spectrum sensing and utilize white spaces of the TV bands. Real time localization which performs better is shown here using RF sensors. The division of Spectrum into N regions gives a high P_D. However, N saturates to a specific value (due to number of averaged PSD's). The lifetime of the network is increased due to less complexity overhead. However, increasing N increases the congestion among the nodes. A suitable strategy is underway.

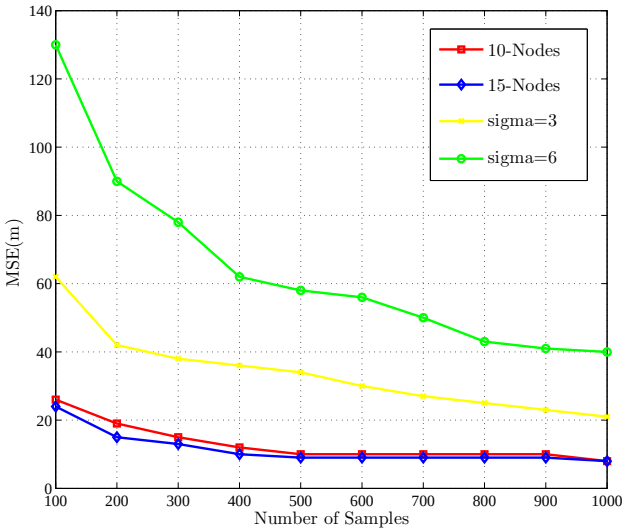

Figure 2.13: MSE Calculation

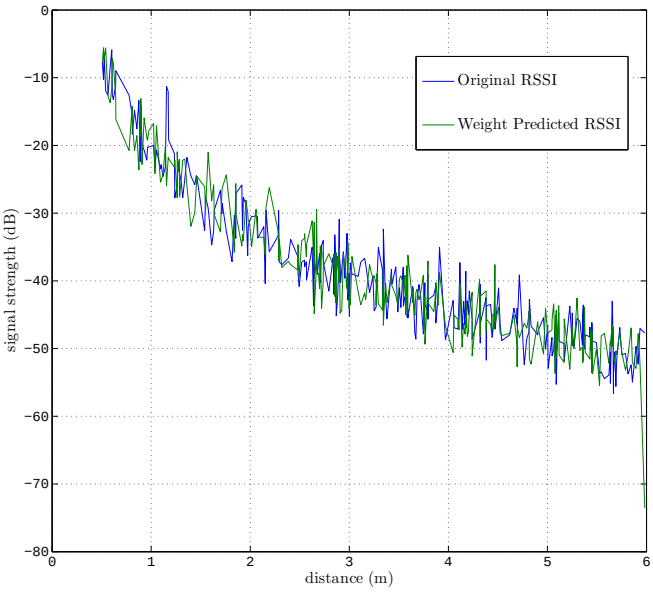

Figure 2.14: RSSI measurements

Chapter 3

Passive Acoustic Localization Scheme

Seaweb network [11] is a wide area network that interconnects the static (Sensor nodes, Buoys, etc.) and mobile wireless nodes (Unmanned Underwater Vehicles (UUV's) Submarines), using Digital Signal Processing (DSP)-equipped telesonar modems [13] and through acoustic links, in the undersea applications. Inter and Intra distances between parent and child nodes are obtained as a byproduct of telesonar signalling and navigation of mobile nodes such as submarines. Link-layer methods like handshaking, selective repeat request (SRQ) and forward error correction provide the network reliability. A network layer mechanism such as maintaining the routing table, feedback packets and packet serialization enhances the quality of service. This scheme uses node-to-node ranges, compiled at parent node, to solve the problem of localization. Synthetic data analysis with different network geometries helps in evaluating the protocol with imperfect ranges, or insufficient data.

Seaweb network basically consists of three main components seaweb server, Gateway Buoy (GB) and repeater/sensor nodes [11]. The seaweb server is located either on the ship or ashore which is inturn controlled by the operator to monitor and control

the undersea deployed network. The GB acts as a centralized node which communicates with all the sensor nodes and thereby improves the lifetime of the network. The GB is the only mode of direct communications from sensor nodes to the server. If there is no direct radio communications between the GB and the nodes then satellite link acts as an alternative way of communication.

The GB is fixed at a suitable position, anchored at the sea/ocean floor, such that it has a direct Line of Sight (LoS) with the seaweb server. The buoy has attached to it the radio/satellite communication equipment and solar panels at its surface. Underwater sensor nodes are usually anchored/moored at the seabed consists of a clamp weight, acoustic release, telesonar Modem and subsurface float [11, 14].

In [15], [16] a technique incorporating the time synchronization between the two nodes without considering the notion of velocity, which increases the error exponentially. However, the complexity of this scheme [15] is high which may result in poor energy efficiency. Moreover, this scheme is very difficult to extend to larger networks. In particular, the number of beacon nodes is set to three in the paper; however, if more than one beacon node is added, then not only program changes are needed for both beacon and ordinary nodes, but also the computational complexity will increase exponentially. However, we try to overcome all the aforementioned problems of reflected paths and watch circles in our scheme and the proposed scheme does not require time synchronization in the network. In [16], the network calculations are implemented by using the ordinary sensor nodes, and we reduce this complexity by incorporating seaweb/GB communication.

In [17], an application of sensor deployment in the Unet'08 seatrial is studied. A fixed speed of sound profile is considered which increases the localization error. This scheme does not take into consideration the displacement of the nodes on the sea surface. We overcome this problem by using Munk's canonical formula [18] and the finite difference linearization and law of cosines.

The chapter is divided as follows. In Section II, we give a brief overview of the seaweb network. This section explains the network layout and the type of protocols being used. Section III, describes the localization algorithm being used and discusses the types of constraints being imposed and its solutions. Section IV, describes the simulations and comparisons of the proposed scheme with the traditional algorithms and finally Section V conclude our chapter.

3.1 Seaweb Network Description

3.1.1 Network Layout

Seaweb network consists of any number of sensor/repeater nodes and GB's. The sensor nodes are interconnected through each other, thereby forming a mesh grid. The paths between each of the sensor node are reconfigurable, if there is a route failure due to the death of the particular sensor. The GB is positioned to maximize its lifetime, i.e. away from the traffic lanes, out of ship, etc. This GB acts as a parent node and also as a relay between the nodes and the server. The term parent is often used to describe the GB as it is localized at the desirable position or it can be used as point of reference (say (0, 0)). Once the GB is deployed, we deploy the first sensor node such that it acts as a second point of reference for the localization purposes. We call this node as ref_x, which is deployed along the line of bearing from the parent node. This allows fixing the location of these two nodes in order to start localization process. The remaining interested nodes are deployed randomly or uniformly as per the interest of the operator. The ranged data is stored into a time-stamped $M \times M$ matrix, where these matrices are complied into time sequenced stacks. This matrix is then statistically analyzed for all the measured ranges between each of the neighbouring nodes, thereby eliminating all the ranges that fall outside a confidence interval of five percent from the mean. These filtered ranges are then

used to localize each of the nodes into x-y position. We then try to form levelling and a mesh network inside levelling, which allows nodes to have multiple communication paths which are reliable. The distance between each of the node is varied from 1 km to 5 km depending upon the deployment and the density of the network.

The acoustic localization/communication has many environmental factors like reflected paths, transmission losses and speed of sound. These factors have been studied in much detail in [11], [12], and [13]. We provide more suitable solutions and a reliable algorithm by taking into consideration these environmental factors.

3.1.2 Network Protocol

Seaweb uses a link-layer protocol for communicating from one node to another for addressing, ranging and power control. A Selective Repeat Request (SRQ) [19] protocol is used for the delivery and the acknowledgment of message units. In this SRQ, nodes use the Request to Send (RTS), and Clear to Send (CTS) command to establish the connection between them before transmitting the data. This is depicted in figure 3.1. The range between the nodes is found by using the PING and ECHO commands (supported by SRQ), which are generated by using the Hyperbolic Frequency Modulated (HFM) signal [20]. When a node x PING to its neighbouring node y, node y determines the time of arrival, (ToA) by using the peak of the HFM matched filter. Node y waits for a specified time (say τ), before sending ECHO to node x, as shown in figure 3.1. This follows the same path based on reciprocity. Henceforth, the sound propagation delays between these nodes are equal ($d_{xy} = d_{yx}$). Once the ECHO is received by node x, seaweb modem calculates the range based on the total time delay as follows;

$$r_{xy} = Cd_{xy} \tag{3.1}$$

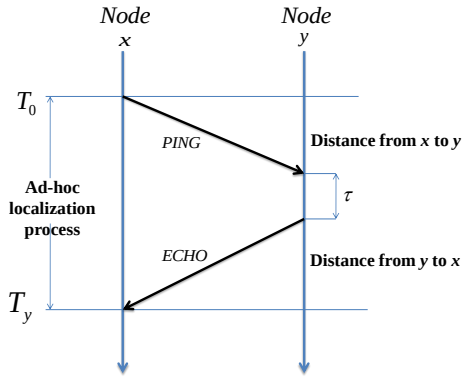

Figure 3.1: Ranging process

where $d_{xy} = (T_y - T_0 - \tau)/2$ and C is the speed of sound and d_{xy} is the distance between node x and node y.

As the depth of sea/water increases the speed of sound varies [21]. Since we use the repeater nodes which are moored at the sea level we consider the speed of sound to be constant at 1520 m/s. However, we consider the cases where the speed of sound varies due to uneven surfaces at the sea bed.

3.1.3 Adhoc Discovery Process

Once the network is deployed the first task is to perform the node-to-node ranges (using PING and ECHO) starting from the parent node and thereby these ranges are maintained at the Seaweb server. Then parent node initiates a PING and commands each of its discovered nodes to conduct the broadcast PING in order to discover the remaining nodes. These nodes thereby maintain the mesh or a route to which they can communicate in a single hop.

3.2 Seaweb Network Passive Localization

Localization in seaweb server of repeater/sensor nodes is done by using range based intersecting circles of the known nodes. When an unknown node (non-localized) comes in contact with two known nodes (localized nodes), it is localized in its x-y plane by using the range based algorithm. In [22] and [23] the weighted averages and center of mass method does not eliminate range errors fully. The finite difference linearization method [16] is proved to be more efficient than compared to other approaches. Based upon the range measurements between the known and unknown sensor nodes there are some constraints which we describe in the following section.

3.2.1 Acoustic Localization Constraints

The localization depends upon the topology of the deployed network and the acoustic nature of the environment. Depending on these scenarios we can have the possible three cases namely; no-sloution, which occurs when there is only one known node range is available for localization. Secondly, many solutions, where one unknown node has two ranges to know known nodes, i.e. there are two ambiguous outcomes that exist when two range circles intersect. However, this can be resolved by using law of cosines [24]. Finally, finite difference linearization [24] is applied, where one unknown node has their range from known nodes, such that a single, unambiguous solution exists.

Acoustic communication does not preserve the variability of different sources of error. Therefore, we need to consider these errors for making the algorithm reliable under non-ideal conditions. Some of the errors are as mentioned below, which has been taken into consideration while designing the algorithm. Appendix I discusses how these errors are taken into consideration.

1. ***Speed of Sound***: It usually varies from 1480 m/s to 1520 m/s, i.e. +1.3% or

-1.3%. We do not presume the speed of sound as 1520 m/s, as the other papers does. We assume that sound travels in a straight line and hence is linearly related to range. However the temperature, pressure, and salinity in the water cause some deviation to the speed of sound which results in refraction. Hence we use a sound speed profile by Munk's canonical profile [28] which is defined as

$$M(z) = C[1 + \varepsilon(e^{-\vartheta} + \vartheta - 1)]\text{m/s} \tag{3.2}$$

where $\vartheta = [2(z - z_{axis})]/S$, C is the speed of light, ε is the perturbation coefficient, z_{axis} is the depth of sound channel, z is the depth of water in meters and S is the scale depth and ϑ is the dimensionless distance beneath the sound channel axis. The values are as defined; z_{axis}=1000 m, $S = 1000$ m, $\varepsilon = 0.0057$ and $C = 1520$ m/s.

2. ***Transmitted/Reflected Paths***: It can result into absorption and scattering that reduces the intensity of sound energy. For the surface, the reduction depends on the roughness of sea surface and the spectral frequency of the transmitted signal [12]. Losses at the bottom are of the order 8 dB per interaction [13]. However, our algorithm takes into consideration these losses when determining the node-to-node ranges by using peak detector filter which allows selecting the highest peak multi-path arrival.

3. ***Node Position or Depth Variance***: It is possible that two nodes are located at uneven surfaces and both of them have a horizontal and a slant range. The horizontal and slant range differences are considered in our algorithm whereby we presume that all nodes cannot be in same horizontal plane.

4. ***Current/Waves Circles***: It is possible that tides can replace the fixed/stationary transducers, thereby causing deviations in the measured ranges and positions of the nodes. These rotations or replacements are called watch circles. Since the transducers are 3 m off the bottom [12] there is a slight variation in the range difference of two nodes.

Algorithm 1: A passive localization algorithm

Input: Set of randomly deployed repeater/sensor nodes
Output: Localization/Mapping of nodes-to-nodes
foreach *Task* m **do**
  foreach *sensor* i **do**
    Calculate Range using SRQ(i,j);
    if *LoS(i,j)* $\neq$ *LoS(j,i)* **then**
      $i = \theta j$;
      $j = \theta i$;
while *non-localized sensor remaining* **do**
  foreach *sensor* m **do**
    Calculate through planar trigonometry, PT(i,m);
    if *PT(i,j)* $\leq$ *PT(i,m)* **then**
      $m = \theta j$;
  Mapping(sensor i on sensor j) ;
for *sensor field* **do**
  Levelling in the sensor field;
  if *Packet from parent node* **then**
    Set level, L1 ;
    Continue until Level, Lm
for *sensors inside the levels* **do**
  mesh grids.

5. ***Dilution of Precision (DOP)***: It occurs when the distance between the two referenced nodes is very close; the triangularized node (unknown node) has a large uncertainty referred to as Geometric DOP or GDOP. However, we tackle this problem by using finite difference linearization.

3.2.2 Localization Algorithm

Localization using the seaweb server consists of basically five steps: Server input, data input, error correction, levelling of the network, mesh grids and finally, determination of location of nodes. The psudocode of our localization algorithm is shown as Algorithm 1.

Step 1: In the first step, the Seaweb server initiates the request to parent node, gateway buoy, to collect all the measure range data with respect to the ref_x node. The ref_x node is placed such that it is in the range of gateway buoy, so that the server may have the true bearing between these two nodes. The operator (at seaweb) then maintains a table which specifies all the measured ranges from repeater nodes.

Step 2: Once the table is ready the data is sorted into a 3D matrix, which contains all the measured ranges. This matrix consists of number of layers equal to the number of range files uploaded by the operator. Each of these layers is a square matrix, where the nodes addresses are placed in the first row and first column of the matrix. Once all the nodes are stacked into the matrix, it is processed for the range errors.

Step 3: In the third step, we analyze the normalized mean error ranges between each pair of nodes. Here each pair of nodes is statistically evaluated which is explained in Appendix I, and the results are stored into a 2D array. We try to put all the ranges of a particular node pair into a single vector, which is obtained from the stacked matrix. Simultaneously, the reciprocal combination (say from node y to node x) is obtained by looking "up the stack".

Step 4: The obtained vector is statistically analyzed between the selective nodes thereby eliminating the error ranges that fall outside five percent confidence interval of the data ranges. Initially, the data that fall outside the 5% Confidence Interval (CI) is noted and its mean is calculated. The datum falling farthest from the mean is eliminated. The mean and CI are then recalculated and the process is repeated until the datum does not fall outside the CI. This final estimate is then stored in a 2D array. This output array is a 2D square array which is symmetric along its diagonal, with node pairs that lack range estimate is denoted as No-Range, NR.

Step 5: This step divides the entire network into circular levels. This is initiated by the parent node. The parent node sends a packet to all its neighboring nodes which are one hop distance away. The nodes receiving the packet from the parent node set their level ID as L1. The ref_x node also has an ID of L1. The L1 nodes inturn increment the packet ID (say L2) and transmits it to its one hop neighbors and these neighbors set their level as L2. The process is continued until all the nodes are levelled in the network. The detail of the process are defined in [25]. After levelling of the network, the nodes try to form the mesh grids/routes from their one hop neighbors. This leads to proactive path formation and thereby decreases the congestion. Figure 3.2 shows the complete process of 5 step implementation in the simulation setup.

Now, once the data has been filtered, averaged and organized into a 2D array, we now estimate the location of the nodes. As explained earlier, the parent node is set to be origin of a horizontal Cartesian grid. The ref_x is placed such that its x-axis is intersecting parent node, coordinates assigned to (ref_x, 0). Once this node is localized, it is considered to be a known node and with the two known nodes the process of localization can be initiated. If there is only one range to the node, it is left isolated unless it has two or more ranges. If there are two known ranges to an unknown node, there exist two solutions. These two solutions are stacked and compared when a previously unknown node becomes known.

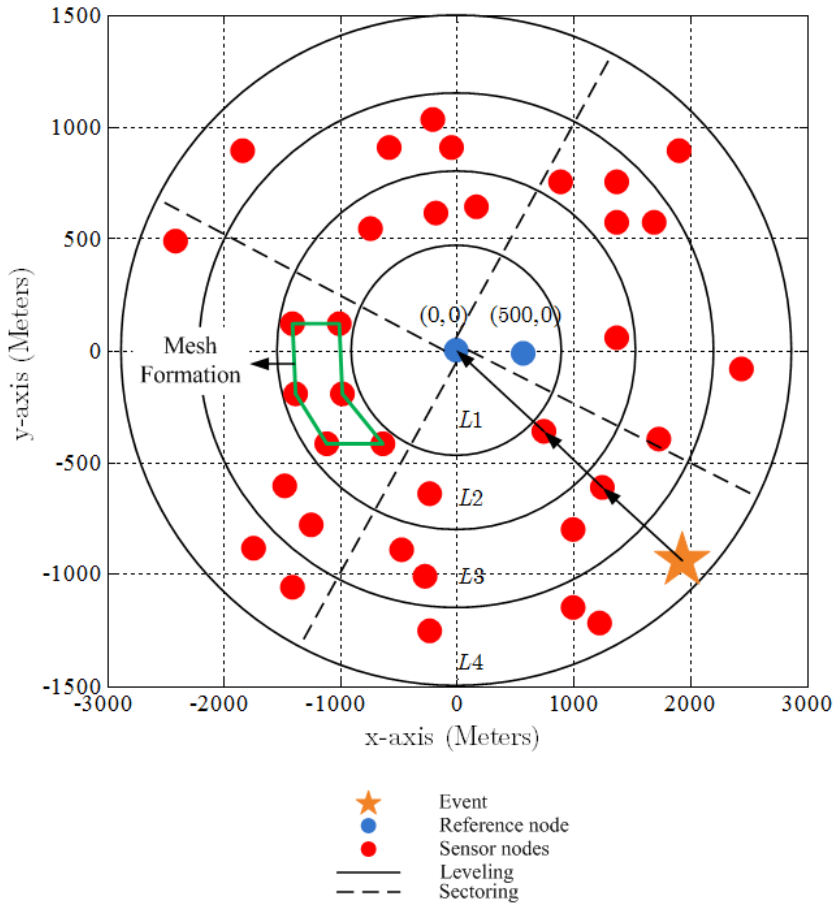

Figure 3.2: Proposed scheme for Seaweb network with circular levels (black) and mesh formation (red). A parent node at (0, 0) and ref_x node at (500, 0) rotated to parent node.

When an unknown node has three known ranges, and then the solution is found using the equation [26] below;

$$\begin{bmatrix} x \\ y \end{bmatrix} = \frac{1}{2} \begin{bmatrix} (x_2 - x_1) & (y_2 - y_1) \\ (x_3 - x_2) & (y_3 - y_2) \end{bmatrix}^{-1}$$

$$\begin{bmatrix} (r_1^2 - r_2^2) + (x_1^2 - x_2^2) + (y_1^2 - y_2^2) \\ (r_2^2 - r_3^2) + (x_2^2 - x_3^2) + (y_2^2 - y_3^2) \end{bmatrix} \tag{3.3}$$

where $[r_i^2] = [(x - x_i)^2 + (y - y_i)^2]$.

If this is for the first time the node is evaluated then we store solution in the stack and loop through all nodes calculation to determine if it is involved in any possible ambiguous solutions sets. If it is not the first time the node is localized then it check with the previous solution. If there x and y coordinate are greater than some threshold difference then the new solution is taken into consideration. This process is continued until all the nodes are perfectly localized into the network.

3.2.3 Routing Protocol

The base idea in this algorithm is to divide the field in to sectors and route the events by using nodes which can switch between SLEEP and WAKE modes.

Step 1 : Levelling

As per our assumptions, we consider a densely deployed sensor field. Initially the Base station sends signals with a minimum power level and all those sensor nodes that receive this information will set their level to one. Then the Base station will increase its power level and transmit the signal. This time those nodes which receive the signal for the first time set their level to two. This procedure continues till all the

nodes in the network have their level ids determined. To counter the effects of fading in wireless channels, hop-count[25] based leveling can also be done.

Step 2 : Sectorization

Using the directional antenna, the Base station will send signals with maximum power and divide the sensor field in to equiangular sectors with an angle of θ (consider θ as 45^o). Now, every node in the network is aware of its level and sector [25].

Step 3 : Clustering or Forming Mesh

Clusters of sensor nodes are formed based on the signal strength and use these local cluster heads as routers to sink. Optimal number of cluster heads is estimated to be 5% of total number of nodes. The decision is made by choosing a random numbers between 0 and 1. The node becomes a cluster head for the current round if the random number is less than the threshold value $T(n)$ which is defined as;

$$T(n) = \begin{cases} \frac{p}{1-p(rmod\frac{1}{p})}, if n \epsilon G \\ 0, otherwise \end{cases} \tag{3.4}$$

Where p is the desired percentage of cluster heads (e.g. 0.05), r is the current round, and G is the set of nodes that have not been cluster heads in last $1/p$ rounds.

Step 4 : Mode Setup

The part of a sector which is in a particular level is called sectroid. If an event occurs in the Level(L), these nodes flood very small metadata packets contain the level id and sector id of the node where the event has occurred (Source node). Each node that receives this packet will read the location of source Levelid (L), if the level of this Levelid is L or $L-2$ or $L-4$ .... then these nodes will go to SLEEP mode. The Levelids with level L-1 or L-3 .. and Level L go to into SLEEP mode.(If and only if there is no transmission in that particular Levelid).

After this setup is completed, the source node floods the data packets in the direction of Base station. The node that receives the packet checks for two conditions,

Table 3.1: Flowchart for Routing Algorithm

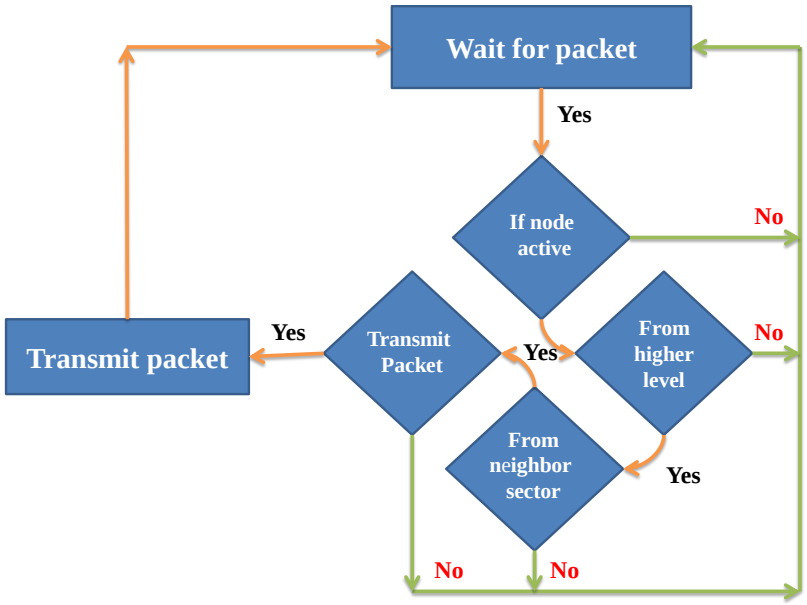

one is the level id and the other is the sector id. If the data is from higher level and it checks for sector id. If the packet is from neighboring sector of higher levels than the packet is forwarded and in other case the packet is discarded.

The proposed algorithm follows this flowchart (figure 3.1) procedure as shown below; 1. When an event occurs at a node, the node floods the data packets to every neighbor. 2. Only the nodes which are in WAKE mode will receive the packet and nodes in SLEEP mode dont receive the packets. 3. Then the nodes that receive data packets check the level id and sector id of the packet. 4. If the level id from the source is lesser than its level id the packet is dropped. 5. If the level id from a source is larger then the node checks whether the sector id is from neighboring sectors i.e. which are at 1 hop distance. If not the packet is dropped.

Table 3.2: Node locations and range estimates.

Node Locations (in Meters)		
Node	*x*-position	y-position
1	4089	4538
25	9877	9874
30	1393	2375
50	7077	5550
70	634	4567

Node-to-Node range (meters)					
	1	25	30	50	70
1	NR	3578	9879	3114	8117
25	3402	NR	987	7664	6774
30	5590	5687	NR	6677	9198
50	2265	2278	7311	NR	8765
70	2451	886	4412	3386	NR

3.3 Simulation Results

In this section, we try to simulate our scheme and then compare the same with the existing algorithms using MATLAB. We randomly generate a 70 node layout on a 10,000 $\times$ 10,000 meter grid, placing the parent node as reference frame axis and ref_x node as $(x, 0)$. The true node locations and range based locations of few selected nodes are given as in Table II.

For realism, GPS devices must be fitted with the most important tool i.e, inertial navigation system (INS). An INS consists of precise accelerometers and gyroscopes to keep track of every change in the mobile sensor node speed and direction. However, ranges exceeding range of 9000 m are neglected (with GPS systems) which inturn are calculated through finite linearization method to delimit the limitations of acoustic communications and to maximize the number of ranges evaluated in each pass. The analysis is carried out for 10 realizations of the 70 node network, resulting in 91,466 ranges being evaluated. The percentage errors between the actual ranges and ranges with offset are recorded. The percentage error between the output and actual ranges are then compared.

The mean percentage error for the range not run through stacks is 5.6%, and the largest percent error is 5.96%. After the ranges are stacked the mean error is reduced

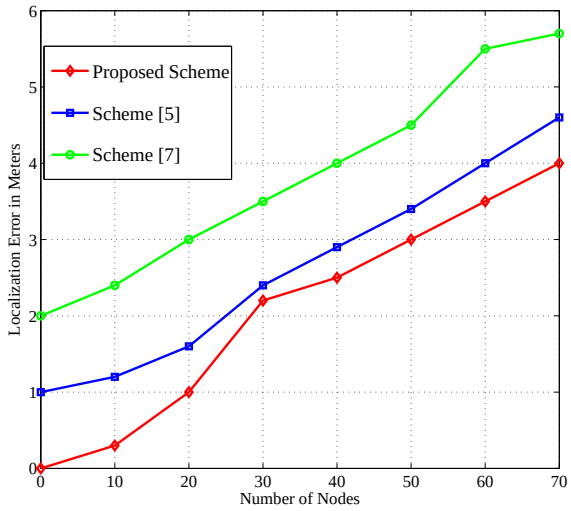

Figure 3.3: Mean localization error for 10 realizations of a 70-node network, using error free ranges. Scheme [7] is referred to [17] and [5] to [15] in the reference section

to 3.5% and the largest percent error is 4.1%. In absolute sense, the accuracy of 10,000 m range estimate is improved by 96.7 m.

Firstly, we perform an error free testing for the algorithm to verify the ability of the proposed scheme to correctly determine the positions of all the nodes in the network. Several statistics are calculated for different network realizations. The most important statistic is how well the algorithm is able to localize the nodes when compares to the actual positions. This is done by finding the normalized mean error for each of the particular node. The mean nodal localization error is 4.6 m with a maximum of 225 m. In [17] the scheme proposed uses a fixed speed of sound profile which increases the localization error. Whereas, [15] uses the time synchronization between the two nodes without considering the notion of reflected paths, which increases the error exponentially. The Fig. 3.3 shows the comparative study made with our proposed scheme. Our scheme performs well and has has least localization error as the number of nodes are increased. However, we notice a peculiar behavior as we try to induce the errors for more than 60 nodes. This surprisingly leads to decrease in the localization error. This scenario is still under investigation.

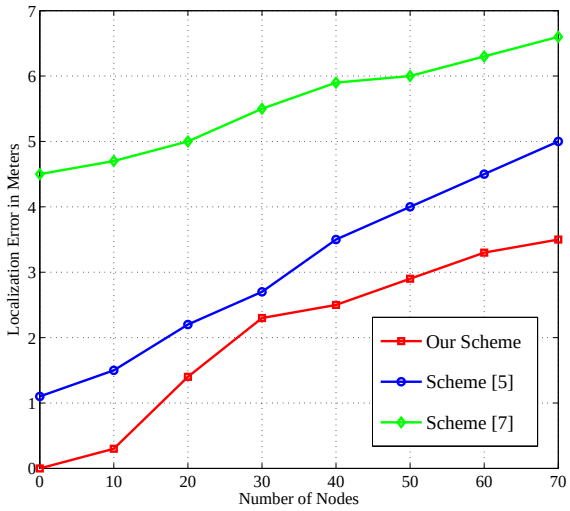

Figure 3.4: Mean localization error for 10 realizations of a 70 node network, using error induced ranges. Scheme [7] is referred to [17] and [5] to [15] in the reference section.

Secondly, in the next set we try to induce the errors using (4) by using the fixed mean and variances. Now, as expected the performance decreases here in case of error-induced ranges. The mean number of nodes localized is 61.5 nodes, shown in Fig. 3.4. As can be seen from Fig. 3.4, addition of bit-errors decreases the localization error, which is opposite to our imagination. Currently, there is no theoretical explanation for this phenomenon. The number of iterations required for the 70 node network to get localized is shown in the next figure. The mean number of iterations for error free ranges is 79.8 whereas the mean number of iterations required for error induced ranges is 140.78 m, Fig. 3.5.

The next figure, Fig. 3.6, shows the number of events detected by the number of the randomly scattered nodes in the network field. An event is any activity detected by the sensor nodes. In this figure, we make a vivid comparison of our scheme with various techniques and methods by George et al and Dough et al. Our scheme proves out to overcome the defect of traditional methods.

In Fig. 3.7 we see the localization estimation error from different target distances.

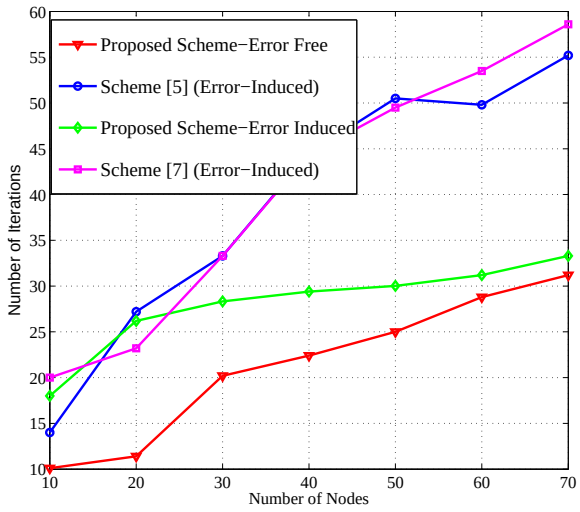

Figure 3.5: Total number of iterations for 10 realizations of a 70 node network. Scheme [7] is referred to [17] and [5] to [15] in the reference section.

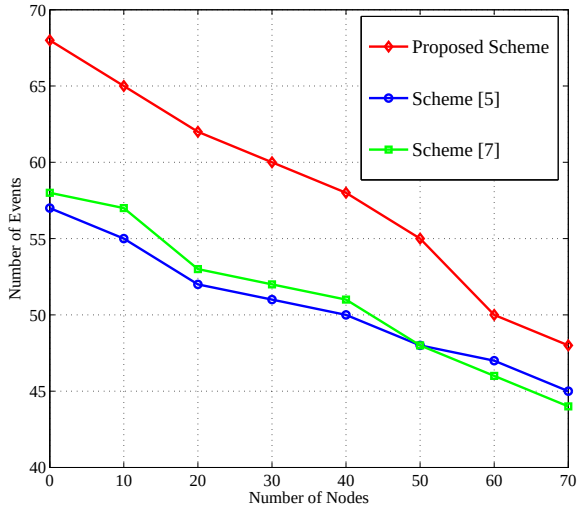

Figure 3.6: Total number of events detection for a 70 node network. Scheme [7] is referred to [17] and [5] to [15] in the reference section.

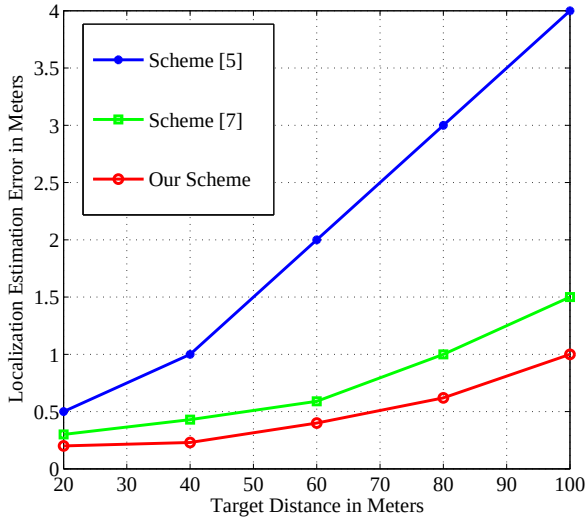

Figure 3.7: Localization Estimation Error with Different Target Distance. Scheme [7] is referred to [17] and [5] to [15] in the reference section.

Our scheme and scheme [15] performs the same with little error difference, this is due to the fact that the base station is considered to be the centralized node. Hence this figures concludes that the localization estimation error increase as the target distance increases.

In Fig. 3.8 we try to make the energy consumption comparison of our proposed scheme with other schemes which proves out that our algorithm requires very less energy consumption as compared to others algorithms. The energy consumptions are calculated per unit time, where the sensors are assigned energy levels and this energy level decreases per unit time as the a sensor tries to detect a event.

In this chapter we thus try to achieve a GPS free localization scheme for underwater sensor networks and the simulation results show that the proposed scheme is energy efficient and is robust. Levelling introduced will help to make the scheme more scalable as adding or removing the nodes does not effect the mesh grids formed inside the levels. Hence, this scheme proves out to be very energy efficient.

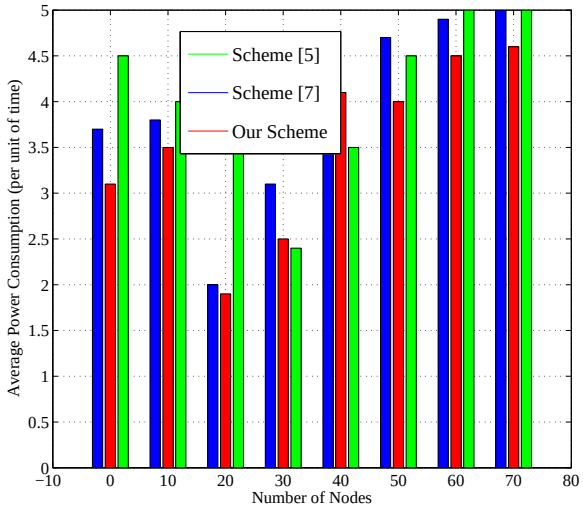

Figure 3.8: Average Energy Consumption per node. Scheme [7] is referred to [17] and [5] to [15] in the reference section.

Chapter 4

3-Dimensional Localization for LTE Femtocell

Wireless Communications demand for higher data rates and has led to the development of new cellular standards like WiMAX (802.16e), the Third Generation Partnership Project's (3GPP's) High Speed Packet Access (HSPA) and Long Term Evolution (LTE) [27], [28]. Femotocell is a small cellular base station (BS), especially designed for home and business areas [29]. Femtocells are low-power, low-cost and user deployed home base stations that can improve poor indoor coverage and enhance system capacity. In 3GGP technology, a Home NodeB (HNB) is a 3G femtocell, whereas, a Home eNodeB (HeNB) is an LTE femtocell. Typically the range of a microcell is less than 2 Km wide, a picocell is 200 m or less, and a femtocell is on the order of 10 m [29].

The two major limitations of wireless communication are range and capacity. Cellular service is far superior in areas of high population density compared to scarcely populated areas. The initial cellular systems were designed for a single application, voice, but today with the advent of fourth generation (4G) cellular systems, users expect good quality of voice, uninterrupted voice calls, clear video images, faster

downloads and precise positioning system. However, the localization of the femtocells subscribers is still an open issue as 4G suffers from inadequate indoor signal penetration, leading to poor coverage in the indoor environment where users spend most of their time. These characteristics indicate that future cellular wireless systems must be designed in a different way, hence the motivation to move towards smaller cells that operate in a licensed spectrum but are privately owned. Femtocells provide a good solution to overcome indoor coverage problems and also to deal with the traffic within Macro cells [30]. The possibility of localizing a femtocells subscriber station based on TRAP [31] within the network signal internals is studied throughout this chapter.

The basic approach to localization based on Euclidean distances from multiple base stations is studied in [32], which proves out to be very energy expensive. We investigate the specification of the timing parameters used for 4G network entry as they relate to calculating the subscriber distances. Computer simulation (using MATLAB) is used to demonstrate expected localization accuracy in multiple base station networks when estimating likely locations of subscriber stations on a three-dimensional coordinate mapping system.

4.1 Proposed Scheme

Femtocells beholds a TRAP or time ranging (TR) parameter similar to GSM and timing adjust (TA) as in WiMAX. The TRAP is the key solution for geolocalization for femtocell subscribers. If the timing of any subscriber needs modification then the network generates a TA command instructing the subscriber to increase or decrease its timing relative to current uplink timing. The user specific TA is transmitted as a (Medium Access Control) MAC control element on the downlink-shared channel (DLSC). In this scheme, we imply the same principles of WiMAX for the knowledge

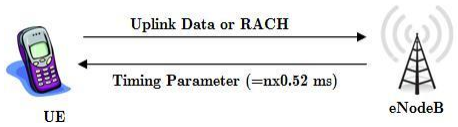

Figure 4.1: Uplink Timing Control.

of signal in relation to TA data to isolate the subscriber location based on the radial distances known to the BS locations.

The TA data is hidden in the transmitted signals and we use the computer simulation to validate and extract this data with multiple BS scenarios under variable conditions such as placing the subscriber at random distances and at random angles from the BS. Femtocells uses several multiple access schemes for uplink and downlink. They are signal carrier frequency division multiple access schemes (SCFDMA) and orthogonal frequency division multiple access (OFDMA) [33]. These schemes allows several subscriber station or user equipment (UE), to share the capacity of the network.

Femtocells uses the two modes of operation for uplink and downlink sharing the same frequency band for transmission and reception: frequency-division duplexing (FDD) and time-division duplexing (TDD). The major difference between the two schemes is the use of paired and unpaired frequency bands respectively. The eNodeB uses the TA control sequence so that the transmissions from the uplink mode arrives within cyclic prefix. The eNodeB continuously measures the timing using random access channel (RACH) of UE uplink signal and adjusts the uplink transmission as shown in Fig. 4.1.

4.1.1 Timing Advance Calculation for Femtocells

A standard 3GGP unit of time is used throughout our calculations and we express the sampling time as, $T_s = 1/(S_s \times FFT_{max})$ Seconds. Where S_s is the subcarrier frequency of 15 KHz and FFT_{max} is the maximum FFT size, which is 2048. We

then divide the radio frame structures of uplink and downlink with duration of T_s and calculate the the radio frame, T_f as a product of T_s and 30.72 MHz sampling frequency such that $T_f = 307200 \times T_s = 10$ ms. Radio frames are subdivided into slots. These slots are expressed in time domain as $T_{slot} = 15360 \times T_s = 0.52$ ms.

3GGP-TS 36.213 standard gives further refinement on transmission timing adjustments, where TA command indicates the change of uplink timings, relative to current uplink timing, in the multiples of $16T_s$. MAC random access responses uses 11-bit TA command T_A indicates N_{TA} values by index values of $T_A = 0, 1, 2, ..., 1282$, then the timing alignment is given as $N_{TA} = 16T_A$. As for N_{TA} this corresponds to the number of TRAP or TA units that need to be applied to the start times of uplink and downlink radio frames and this gives a maximum of 20512 TA units. In some cases, 6-bit TA command indicates adjustment of the current N_{TA} value $N_{TRAP,old}$ to the new T_A value $N_{TA,new}$ where we define $N_{TA,new} = N_{TA,old} + 16(T_A - 31)$ where $T_A = 0, 1, 2, ..., 63$. It is observed here that adjustment of N_{TA} by a positive or negative amount indicates the increase or decrease of uplink transmission timing by a certain amount. With this calculation one can achieve the time and distance with respect to one unit of TA. Literature review predicts the value of TA as 0.67 ms [34] correlating to radial distance of 100 m from eNodeB to UE. For correctness of this value we used the formula as below;

$$N_{TA} + N_{TAoffset} \times T_s = (20512 + 0) \times 1/(15000 \times 2048) = 0.672ms \tag{4.1}$$

The distance for per unit of TA is derived using the sampling frequency of 3GGP. Different sampling frequencies are listed in [34]. Then we calculate the final distance as, Distance $= (c/f_s)$, where c is the speed of light. Then each unit of TA should correlate to a distance of 78.14 m. The maximum index value (1282) when multiplied

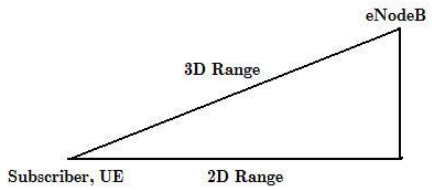

Figure 4.2: 2D and 3D localization ranges.

by 78.14 m produces a distance of 100.17 Km, thereby validating the assertion found in literature. In our simulation model we apply this calculated distances to normalize the intersecting radii.

4.1.2 Approach for Range Approximations

In this section, we try to derive the approximations needed for calculation of the 3D distance between eNodeB and UE as shown in Fig. 4.2. Since, eNobeBs and UE uses the TA-based radius which proves out to be more precise than 2D coordinate system. The illustration of the difference between 2D and 3D is shown in figure 4.2. However, the z-axis varies between UE and eNodeB and hence it leaves an error. We try to employ the method of triangulation for determining the relative position of UE's from respective eNodeB. 3D approximations requires the trilateration of spheres rather than circles as in 2D case. This technique is used by GPS, where satellite in space acts as a center point for the spheres. The estimated point of intersection of three or more satellite spheres gives the likely location of the GPS device. For calculating the 3D ranging we need to determine the height(z-axis) from the center of the sphere of the eNodeB.

In range approximation we employ three parameters. Firstly, we employ a flat earth model whose calculation are based on Cartesian coordinates [35]. This provides a coordinate system with simplified calculations of range radii, intercept points and probability polygons. The flat model's typical error over the geode is very small even after a coordinate transformation. Secondly, intersecting radii is based on the

propagation delay of the signals, as calculate in the section above. The range radii calculations uses a the best scenario with an absolute TA by amount of 78.14 with no variance and standard deviation The last parameter offsets the best case scenario by using deviation of range radii calculations. The study of 3GGP specifications leads us to the establishment of real-world value of deviation as 78.14 m.

4.1.3 Node Location Calculations

With two eNodes having the known radius the likely location of an UE is the point of intersection of radius rings. Here we take into account the three possible scenarios; two radius of spheres are separated without touching, one sphere completely inside another and radius sphere that intersect each other. When two spheres intersect then there is an additional plane with vast number of intersection points. Henceforth, we introduce a third sphere to calculate the point of intersection that localize the UE.

We developed a algorithm using triangulation and law of cosines and we found spheres from eNodeBs using the TA-based radii, $X-Y$ plane coordinated of eNodeB and height of the eNodeB as on z-axis. This leads to a system of equations we used using linear algebra to determine the most common point of intersection. The Cartesian coordinates of the i-spheres equate to a system of following equation

$$(x - x_i)^2 + (y - y_i)^2 + (z - z_i)^2 = R_i^2 \tag{4.2}$$

where (x_i, y_i, z_i) corresponds to the intersecting center points of the spheres with R_i as the corresponding radii, calculated from [34] by using law of cosines and i represents the number of femtocell base stations. Once we substitute the values of center points and radii (for $i = 4$) we further reduce the system by subtracting the equation of first sphere from the equations of remaining two spheres. we obtain the following set of equations

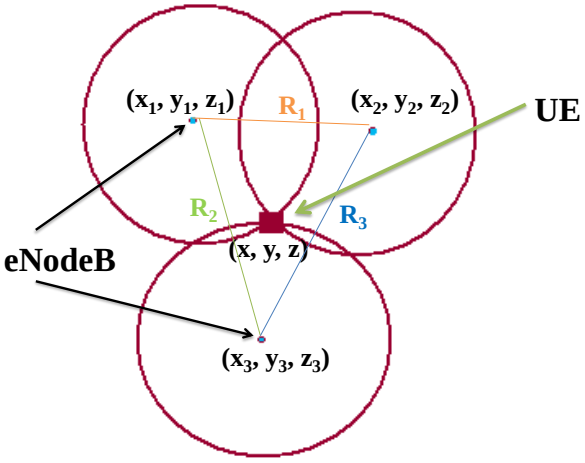

Figure 4.3: Node locations in 3D sphere scenario.

$$
\begin{aligned}
2[(x_2 - x_1)x + (y_2 - y_1)y + (z_2 - z_1)z] &= d_1 \\
2[(x_3 - x_1)x + (y_3 - y_1)y + (z_3 - z_1)z] &= d_2 \\
2[(x_3 - x_2)x + (y_3 - y_2)y + (z_3 - z_2)z] &= d_3
\end{aligned} \tag{4.3}
$$

$$
\begin{aligned}
d_1 &= R_1^2 - R_2^2 - x_1^2 + x_2^2 - y_1^2 + y_2^2 - z_1^2 + z_2^2 \\
d_2 &= R_1^2 - R_3^2 - x_1^2 + x_3^2 - y_1^2 + y_3^2 - z_1^2 + z_3^2 \\
d_3 &= R_2^2 - R_3^2 - x_2^2 + x_3^2 - y_2^2 + y_3^2 - z_2^2 + z_3^2
\end{aligned} \tag{4.4}
$$

To find the common point of these intersection sphere we define a linear transformation of the form $\mathbf{A}x = b$. This is portrayed as

$$2\begin{bmatrix} (x_2-x_1) & (y_2-y_1) & (z_2-z_1) \\ (x_3-x_1) & (y_3-y_1) & (z_3-z_1) \\ (x_3-x_2) & (y_3-y_2) & (z_3-z_2) \end{bmatrix}\begin{bmatrix} x \\ y \\ z \end{bmatrix} = \begin{bmatrix} d_1 \\ d_2 \\ d_3 \end{bmatrix}$$

where matrix $\mathbf{A}$ holds the coefficients and b holds the constants from (3) and x are the unknown coordinates for the intersection (x, y, z).

The unknown point is calculated as $x = \mathbf{A}^{-1}b$. But the inverse of matrix is possible only for square matrix. When A is not a square matrix we find the solution by using the least squares or best-fit-in solution by using normal equation, $\mathbf{A}^T\mathbf{A}x = \mathbf{A}^T b$, which gives a unique solution $\hat{x} = (\mathbf{A}^T\mathbf{A})^{-1}\mathbf{A}^T b$ and $\hat{x}$ is the unique solution to least squares method. In the following section we use the following results to simulate our cased for multiple BS.

4.2 Simulation Results

In this section, we try to study our model for three BS, four BS and for multiple BS. In this first approach we use 3 eNodeB radii to approximate the location of a UE. In all cases the true position of the UE's is set at origin on the $X - Y$ axis. The simulation creates eNodeB at varying degrees each with normally distributed at random distance with a mean of 1 Km from UE and a standard deviation of 300 m and the TA is maintained at 78.14 m. TA being a discrete value the eNodeB rounds the radial distance to whole unit of TA. A monte carlo simulation of 1,00,000 iterations were conducted for each with an degree increment of 10 degrees ranging from 0 to 180 degrees.

We observe that most accurate approximation of the UE location occurs at 180 degrees when the placement of the eNodeB and the UE form a straight line with each other. Tower height of the eNodeB was generated with normally distributed random

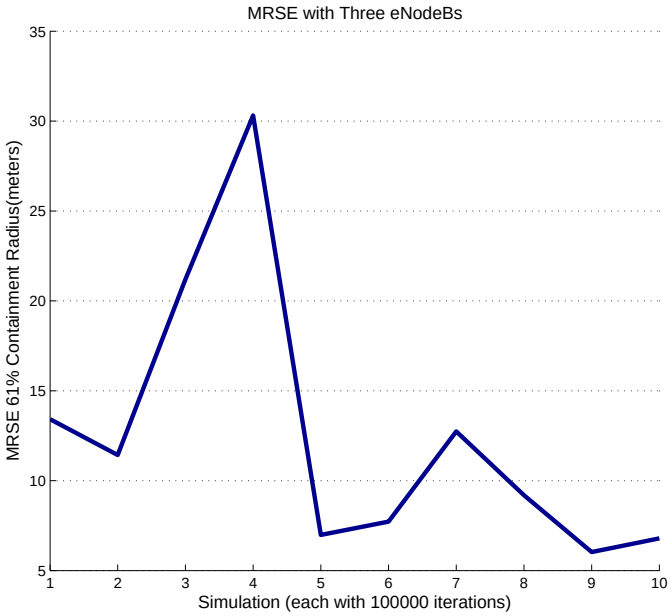

Figure 4.4: MRSE.

heights with a mean of 300 m from the ground plane with a standard deviation of 250 m to facilitate a minimum eNodeB height of 50 m. Trials from Monte Carlo were recorded and we then apply the quantization error. In this case the accuracy was tested and compared with the simulation results without errors. We observe that standard deviation to TA and quantization error to radii had little effect on the approximation error.

A mean radial spherical error (MRSE) analysis was also conducted and the results are shown in Fig. 4.4 and Fig. 4.5. MRSE is calculated by summing the variances of X, Y and Z coordinates of all 1,00,000 Monte Carlo simulations and the square root value is obtained. The radial value of MRSE centered on the origin and the actual UE location shows 61% of the location values are contained. An estimate error for multiple femtocell stations is studied in these graphs.

The next simulation investigates the case for 4 eNodeB network. The same parameters are used that were used for 3 eNodeB network. With the addition of the fourth node the location accuracy increases and is shown in Fig. 4.7.

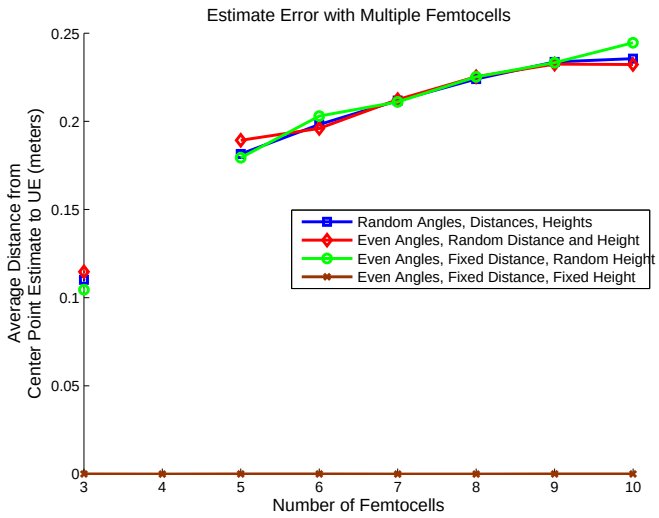

Figure 4.5: MRSE.

The final simulation is done for multiple eNodeB, as shown in Fig. 4.6, and inturn test the approximation accuracy. First eNodeB were placed in random random angles in relation to the UE at the origin. Distances of eNodeB is 1.2 Km with a standard deviation of 400 m. Tower heights are generated with a mean of 300 m and with a standard deviation of 250 m, which facilitate the height of 50 m. The largest approximation error occurs with 4 eNodeB network but the margin of approximation error with five or more nodes remained consistent despite of the additional tower heights. This leads to an interesting fact that a system of equations is precise in case of 2 eNodeB.

In this chapter, we try to find a very efficient way to localize the 4^{th}G network subscribers. We mainly concentrate on femtocells that have a good range of coverage. Timing advance parameters can be useful to achieve the synchronization between uplink and downlink communication. Triangularization can be very helpful to find the a unique solution for 3-Dimensional coordinate system. The accuracy of using this method is show in the results. This developed scheme can be further extended to picocell or macrocell provided we have correct calculations of TRAP.

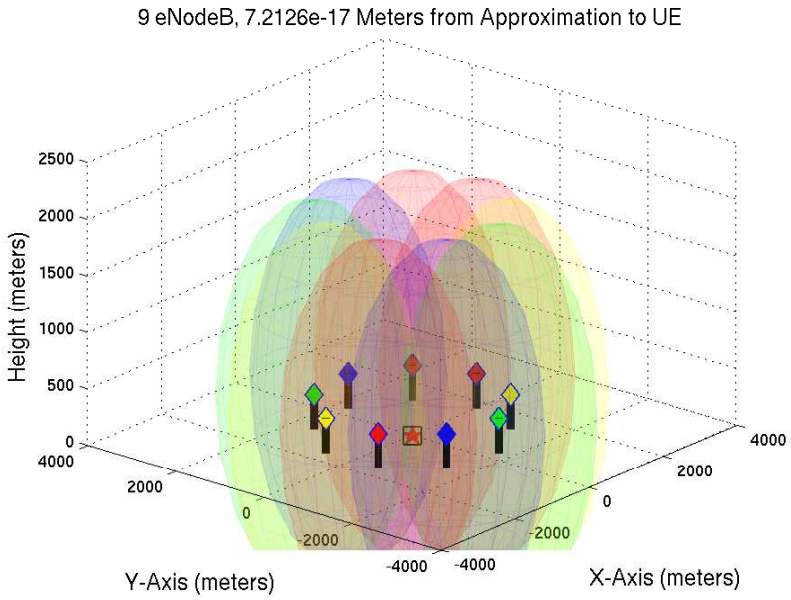

Figure 4.6: Example of accurate location estimate with 9eNodeB network.

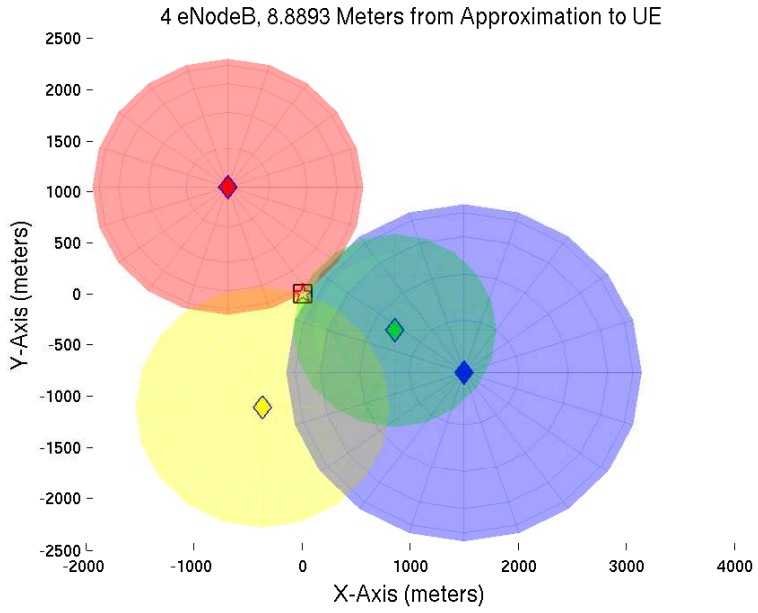

Figure 4.7: 4 Femtocells with an UE. (where *rhombus* represent the femtocell BS and *square* is femtocell subscriber station location and *star* represents the actual calculated position of eNodeB)

Chapter 5

CONCLUSIONS

In chapter two, Our simulation results show that the proposed LCC spectrum sensing method using RF sensor networks performs well in detecting available frequency bands and finding the transmitter base station locations within the network range. The implementation successfully integrated wavelet-based MRSS with N-bit hard combination and RSS-based localization to do the task. The simulation results show that the more nodes that are used in the cooperative sensing, the better the detection capability of the network. However, at some point (around 15 to 20 nodes), increasing the number of nodes does not improve the performance anymore. This is mainly because we reach the maximum P_D. The same patterns can be observed from the number of averaged power spectral densities (PSD's). The results also show that increasing noise levels decrease the detection accuracy of the sensor network but increasing the number of averaged PSD's improves the performance to overcome the low SNR. It was also shown that in terms of detection accuracy, 4-bit hard combination outperforms 2-bit and 3-bit hard combinations. The benefit of using N-bit hard combinations (with $N > 2$) was also illustrated by showing that the probability of false alarms decreases as N increases. Finally, the RSS-based localization technique shows a fairly accurate distance measurement based on the results.

In chapter three, we have presented a simple acoustic underwater protocol and implement the same for the existing algorithms. We overcome the problems of watch circles by using Munk's formula and by averaging the signal. When we apply the criterion of levelling it is observed that the performance evaluation has been increased and mesh networks typically, for the proactive routes, avoids the traffic control paths. The comparison of our proposed scheme with that of the traditional approaches proves our scheme to be energy efficient and improves the localization capabilities. The localized scheme proves out to be robust and has less storage (of node positions) overhead and complexity. Future works include improving the algorithm by overcoming the error uncertainties caused by ambiguous solutions. We also plan to incorporate a partition strategy such that it reduces the total number of iterations and the accumulative errors.

For future work, an FFT-based MRSS can be implemented to see if it has performance advantages over wavelet-based MRSS. In addition, other estimation parameters such as time of arrival (TOA), time distance of arrival (TDoA) or angle of arrival (AoA) or a combination of any of these parameters can be used for localization instead of RSS only.

In chapter four, we investigate and come up with a geolocalization technique for femtocell subscribers. We propose a novel technique of triangulation and localization among UE's and eNodeB and UE's. The use of novel triangulation technique improves the accuracy of the location exponentially for a 3D coordinate system. The main idea of geolocalization hides in knowledge of TA values and offset and tower characteristics of eNodeB. Our approach proves out to be more efficient and can geolocate the femtocell subscriber within 3 m of range (can be inferred from the figure 4.6).

APPENDIX

Synthetic Analysis of Datumn

Synthetic data is generated in MATLAB using the built-in command 'unidrn' function that gives uniformly distributed coordinates of the nodes. Error free ranges, r_{true} are calculated by node pairs where as error induced ranges are generated by;

$$r_{error-induced} = \mathcal{N}(\mu, \sigma) \times r_{true} + 0.02 \times r_{true} \times \chi^2(\theta) \tag{5.1}$$

where we multiply by normally distributed random variable (rv) by error-free range and then adding 2 % of the error-free range multiplied by chi-squared distributed random varible. The normal distribution accounts for speed of sound errors which are proportional to range of the nodes. The mean, μ and the variance, σ of the normally distributed rv is set to 1 and 0.01 respectively, to ensure that reported ranges are near actual range. Moreover, the chi-squared distribution, $\chi^2(\theta)$ is used to account for the reflected transmission paths and depth variance errors, which are also proportional to range of the nodes where θ is the degree of freedom and the mean and variance is set to 1 and 4 respectively. When it is multiplied with 10% of the error-free range, it results in 10% overestimation of the range. Watch circles are addressed by typically averaging out over the course of network operation.

REFERENCES

[1] Y. Zeng, Y. C. Liang, A. T. Hoang, and R. ZhangH, "A review on spectrum sensing techniques for cognitive radio: challenges and solutions", *Eurasip Journal on Advances in Signal Process*, January 2010.

[2] Y Carlos Cordeiro, Monisha Ghosh, Dave Cavalcanti, and Kiran Challapali, "Spectrum Sensing for Dynamic Spectrum Access of TV Bands (Invited Paper)", *ICST CrownCom*,Orlando, Florida, August 2007.

[3] J. Vartiainen, J. Lehtomki, H. Saarnisaari, Juntti; Umebayashi, Kenta, "Two-Dimensional Signal Localization Algorithm for Spectrum Sensing", *IEICE Transactions on Communications*, Volume E93.B, Issue 11, pp. 3129-3136, 2010. .

[4] J. Shirahama and T. Ohtsuki, "RSS-based localization in environments with different path loss exponent for each link", *IEEE Vehicular Technology Conference*, pp. 1509-1513,Calgary, Alberta, 2008. .

[5] Q. Zhang, "Cognitive Radio on a Reconfigurable MPSoC Platform", *PhD Dissertation*, University of Twente, Netherlands, February 2009. .

[6] J. Park, T. Song, J. Hur, S. M. Lee, J. Choi, K. Kim, J. Lee, K. Lim,C. H. Lee, H. Kim, and J. Laskar, , "A fully integrated UHF receiver with multi-resolution spectrum sensing (MRSS) functionality for IEEE 802.22 cognitive radio appli-

cations", *IEEE International Solid-State Circuits Conference*, Francisco, California, February 2008. San .

[7] J. Park, Y. Hur, T. J. Song, K. W. Kim, J. Lee, K. Lim, C. H. Lee, H. Kim, and J. Laskar, 'Implementation issues of a wideband multi-resolution spectrum sensing (MRSS) technique for cognitive radio (CR) systems", *IEEE First International Conference on Cognitive Radio Oriented Wireless Networks Communications (CrownCom2006)*, pp. 1-5, Mykonos Island, Greece, June 2006.

[8] J. Ma, G. Zhao, Y. (Geoffrey) Li, "Soft Combination and Detection for Cooperative Spectrum Sensing in Cognitive Radio Networks", *IEEE Transactions on Wireless*, vol. 7, pp. 11, November 2008. .

[9] J. Mitola, J. Maguire, G. Q., "Cognitive radio: Making software radios more personal", *IEEE Personal Communications*, vol. 6, pp. 13-18, August 1999.

[10] V. Somenzer, "Cooperative Wideband Spectrum Sensing and Localization", *Graduate Thesis*, NPS, California, USA, September 200. .

[11] G. N. Roberts, and R. Sutton, "Advances in unmanned marine vehicles", *Institution of Electrical Engineers*, 2006.

[12] J. Rice, "Seaweb acoustic communication and navigation networks", *Proceedings of the International Conference"Underwater Acoustic Measurements: Technologies & Results"* June 2005. Crete, Greece.

[13] Benthos Inc., "Acoustic telemetry modem ATM-885", *(www.benthos.com)*.

[14] K. Scussel, "Acoustic modems for underwater communications", *Wiley Encyclopedia of Telecommunications*, vol. 1, pp. 15-22, Wiley-Interscience, 2003.

[15] W. Cheng, A. Thaeler, X. Cheng, F. Liu, X. Lu, and Z. Lu, "Time synchronization free localization in large scale underwater acoustic sensor networks",

IEEE Conference on Distributed Computing Systems Workshops, June, 2009. Qubec, Montreal.

[16] T. S. Schei,"A finite-difference method for inearization in nonlinear estimation algorithms", *Automatica*, vol. 33, Issue 11, Novermber 1997.

[17] G. J. Dough, "Undersea communication network self-localization during the Unet'08 seatrial", *Oceans 2010, MTS/IEEE Biloxi - Marine technology for our future: global and local challenges.* Biloxi, Mississippi.

[18] W. H. Munk, "Sound Channel in an exponentially stratified ocean, with application to SOFAR", *Institute of Geophysics and planetary Physics*, Scripps Institution of Oceanography, 1974.

[19] K. Ausavapattanakun, "Analysis of selective-repeat ARQ via matrix signal-flow graphs", *IEEE transactions on Communications*, vol. 55, no. 1, January 2007.

[20] J. Yang and T. K. Sarkar, "Acceleration-invariance of hyperbolic frequency modulated pulse compression", *Digital Signal Processing* vol. 18, issue 2, Pages 228-235, March 2008, Mykonos Island, Greece.

[21] G. N. Roberts, R. Sutton, "Advances in unmanned marine vehicles", *Institution of Electrical Engineers - Technology and Engineering*, 2006.

[22] K. Scussel, "Acoustic modems for underwater communications", *Wiley Encyclopedia of Telecommunications*, vol. 1, pp. 15-22, Wiley-Interscience, 2003.

[23] S. P. Ouimet, "Undersea navigation of a glider UUV using an acoustic communications network", *M.S. Thesis, Naval Postgraduate School.* September 2005. California, USA.

[24] The Math Page, "Proof of Law of Cosines", http://www.themathpage.com/aTrig/law-of-cosines.htm.

[25] M. A. Mirza, R. Garimela, "PASCAL: power aware sectoring based clustering algorithm for wireless sensor networks", *The International Conference on Information Networking (ICOIN)*, January 20-24th, 2009. Chiang Mai, Thailand.

[26] L. O. Krause,"A direct solution to GPS-type navigation equations", *IEEE Transactions on Aerospace and Electronic Systems*, vol. AES-23, pp.224 - 232 , 1987.

[27] E. Dahlman, S. Parkvall, J. Skold, and P. Beming, "3G Evolution: HSPA and LTE for Mobile Broadband", *Elsevier Ltd., Second Edition"*, Burlington, Massachusetts, 2008.

[28] S. Sesia, I. Toufik, and M. Baker, "LTE-The UMTS Long Term Evolution From Theory to Practice", *West Sussex, United Kingdom: John Wiley and Sons Ltd.*, 2009 .

[29] V. Chandrasekhar, and J. G. Andrews, "Femtocell Networks: A Survey", *IEEE Communications Magazine*, vol. 46, Issue 9, September 2008.

[30] Y. Shi, MacKenzie, DaSilva, Ghaboosi, and Latva-aho, "On Resource Reuse for Cellular Networks with Femto- and Macrocell Coexistence", *2010 IEEE Global Telecommunications Conference, GLOBECOM 2010*, Miami, Florida, December 2010.

[31] M. A. Spirito, and A. G. Mattioli, "Preliminary experimental results of a GSM mobile phones positioning system based on timing advance", *in IEEE Vehicular Technology Conference*, vol. 4, pp. 2072-2076, Amsterdam, Netherlands, September 1999. .

[32] H. Breu, J. Gil, D. Kirkpatrick, and M. Werman, "Linear time Euclidean distance transform algorithms", *IEEE Transactions on Pattern Analysis and Machine Intelligence*, Vol. 17, Issue 5, pp. 529-533, May 1995.

[33] G. Berardinelli, L.A. Ruiz de Temino, S. Frattasi, M. Rahman, and P. Mogensen, "OFDMA vs. SC-FDMA: performance comparison in local area IMT-A scenarios", *IEEE Wireless Communications*. vol. 15, Issue 5, pp. 64-72, October 2008.

[34] Agilent Technologies, "LTE-DL-Src (Downlink Baseband Signal Source)", *Institute of Geophysics and planetary Physics*, [Online], 2010.

[35] T. S. Schei, "A finite-difference method for inearization in nonlinear estimation algorithms", *SINTEF Electronics and Cybernetics*, Vol. 19, Issue 3, pp. 141-152, Novermber 1998.